

Alluvial* gold potential in buried palaeochannels in the Wyalong district, Lachlan Fold Belt, New South Wales

Kenneth C. Lawrie¹, Roslyn A. Chan², David L. Gibson², & Nadir de Souza Kovacs³

Recent advances in understanding palaeodrainage in regolith terrains have led to the development of new conceptual models for landscape evolution in the **Lachlan Fold Belt**. At the same time, new high-resolution airborne geophysical datasets (magnetic, γ -ray spectrometric, and electromagnetic, AEM) have helped delineate many regolith features with no surface expression — notably buried, alluviated palaeoriver channels. Such palaeochannels, mainly in areas adjacent to high ground, were identified in the 19th century in several of the goldfields in the Lachlan River catchment, where some were mined for alluvial gold and tin until the early 20th century. We have delineated previously unrecognised palaeochannels on high-resolution magnetic images near the Wyalong Goldfield, an historic source of primary gold in quartz veins. Some of these newly dis-

covered palaeochannels may be prospective for alluvial gold sourced by erosion of the vein deposits.

Geomorphic and palaeogeographic setting

The Wyalong Goldfield is adjacent to the western margin of the north-south-trending Bland Creek palaeovalley (130 × 60 km; Fig. 1), which controlled the northward flow of Tertiary palaeorivers discharging into the main westward-flowing palaeo-Lachlan River system. The palaeovalley drainage first incised (probably in the Paleocene) an already weathered terrain in which saprolite profiles in bedrock locally extended 50 m or more deep. Time-transgressive incision proceeded by nickpoint retreat in response to the combined effects of differential uplift associated with continental break-up, downwarping of the Murray Basin,

and likely climate control related to eustatic sea-level changes (Gibson & Chan 1999: 'Proceedings of Regolith 98 Conference, Kalgoorlie, May 1998', CRC LEME, Perth, 23–37).

Drilling and seismic refraction profiling show that the Bland Creek palaeovalley has a crudely asymmetric cross-section owing to more pronounced incision on its eastern side (Anderson et al. 1993: *NSW Department of Water Resources*, Technical Services Report 93.045). North-northwest-trending ridges in the palaeovalley apparently owe their expression to bedrock composition, including alteration/mineralisation overprints. On the western palaeovalley margin, numerous magnetically delineated ENE- to NNE-trending palaeochannels appear to cut through these ridges. Steep-sided palaeochannels (gorges?) underlying the Temora Goldfield are as deep as 140 m (Lishmund 1972: Records of the *Geological Survey of NSW*, 14(2), 133–157).

Alluviation of the palaeo-Lachlan River system during the late Tertiary (Williamson 1986: *Water Resources Commission, NSW, Hydrogeological Report 1986/12*) buried the Bland Creek palaeovalley, whose alluvial fill comprises two formations. The Late Miocene to Pliocene Lachlan Formation — quartz-dominant, poorly sorted sand and gravel to cobble size — was deposited in a swampy, moderately reducing environment. After a brief erosional hiatus, the Pleistocene Cowra Formation, brown gravel and clay, accumulated in a more oxidising environment in which gravel distribution across the palaeovalley indicates constant reworking by braided stream channels (Williamson 1986: *op. cit.*).

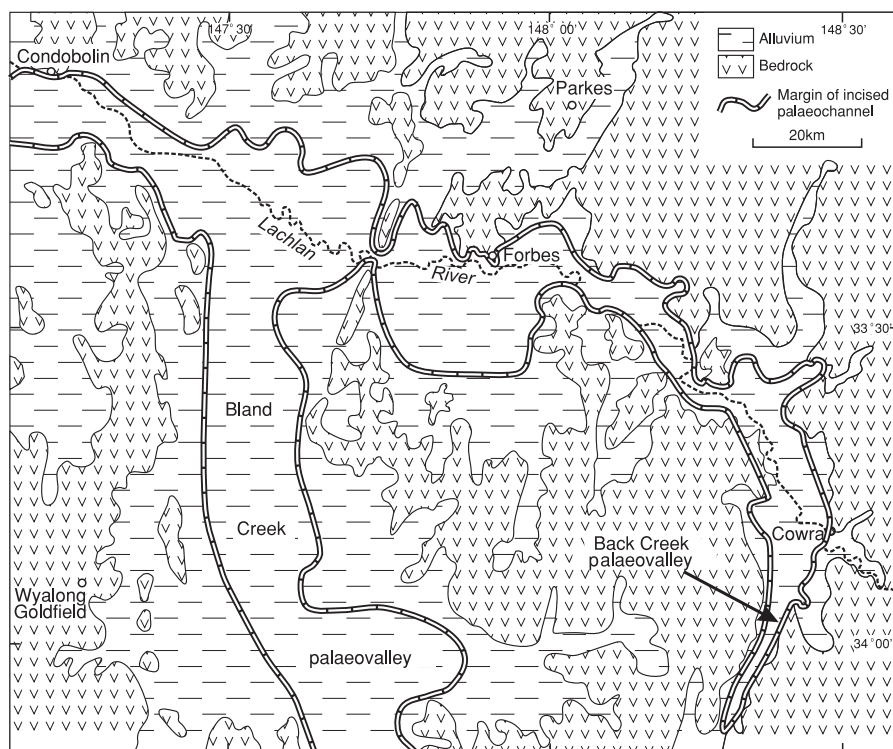


Fig. 1. The Bland Creek palaeovalley in relation to the Lachlan River and Wyalong Goldfield.

* We use the term 'alluvial' synonymously with the terms 'placer', 'palaeoplacer', 'lead' and 'deep-lead'.

Alluvial gold associated with the Lachlan River and Bland Creek palaeovalleys

Gold from alluvial palaeochannels contributed greatly to total gold production from several goldfields in the Lachlan River and tributary Bland Creek palaeovalleys. For example, 3.8 out of 4.2 t Au was mined from the alluvial workings in the Temora Goldfield (Lishmund 1972: op. cit.), ~60km south of Wyalong.

Basal units in the Lachlan Formation are the principal source of alluvial gold in the palaeochannels. The auriferous sediments are typically 0.5–2 m thick and up to 100 m wide (Andrews 1910: NSW Geological Survey Report, Mineral Resources 13; Wilson & McNally 1996: 'Symposium on the geological evolution of eastern Australia', Sydney University Consortium of Geology and Geophysics, 71–73), but appear to be less continuous laterally and downstream than those in palaeochannel deposits in Victoria (Nielsen 1998: Australian Institute of Geoscientists [AIG] Bulletin 24, 121–125). Gold within leads was mined up to 6 km downstream of the channel heads (Mullholland 1935: NSW Geological Survey, Report 1935/002; Lishmund 1972: op. cit.). Only in a few examples was it recovered from horizons higher up than 2 m in the palaeochannel fill (e.g., at Golden

Gate, Temora; Lishmund 1972: op. cit.).

Lateral gold distribution in the palaeochannels is complex. It apparently was controlled by a combination of fluvial processes and local channel geometry. Gold was mined from tributary channels, and at the junction of tributaries and the main channel in the Temora Goldfield (Lishmund 1972: op. cit.). Other examples of local controls on gold grades include 'depressions' or scour holes in the courses of channels, and bends in creeks within the main palaeochannel 'gutters' (Andrews 1910: op. cit.; Lishmund 1972: op. cit.).

Chemical dissolution and reprecipitation of gold in alluvial deposits may have been important for redistributing gold within some deposits in the Bland Creek palaeovalley. For example, high gold grades were associated with limonite-cemented gravels in palaeochannels at Temora (Lishmund 1972: op. cit.).

The Wyalong Goldfield — potential source for alluvial Au

The Wyalong (and Hiawatha) Goldfield (Fig. 2) occupies a mainly erosional terrain in which colluvium and alluvium associated with modern drainage form a thin veneer (<3 m) over much of the saprolitic bedrock. Relief in the Wyalong

area is subtle, and it is difficult to distinguish between the mostly erosional terrain and the surrounding alluvial areas.

Between 1894 and 1920, the Wyalong goldfield produced ~14 t (450 000 oz) Au (Bowman 1977: 'Forbes 1:250 000 mine data sheets and metallogenic study', NSW Geological Survey, Report) — all of it from several narrow north-northeast-trending subparallel veins (Watt 1899: NSW Geological Survey, Report, Mineral Resources 5; Bowman 1977: op. cit.).

Prospectors initially discovered the location of individual auriferous veins in this area by tracing gold-bearing quartz float up very low-gradient slopes in dense mallee scrub. The lack of alluvial gold was attributed to the difficulty of prospecting for such deposits in flat country (Pittman 1900: Department of Mines, NSW, Annual Report for 1899, 164). Pittman surmised that the area was denuded in Tertiary times, and that higher rainfall in previous times had conspired with the district's elevation to form drainage channels. Others discounted the formation of alluvial prospects owing to the fine grain size of the gold, which they asserted would have been dispersed by aeolian processes in a moderately arid environment (Watt 1899: op. cit.). Lack of relief, low rainfall, and scarcity of groundwater for supporting sluicing operations (Lishmund 1972: op. cit.) also dampened enthusiasm for alluvial-gold prospecting in the Wyalong area.


Early mining, nevertheless, revealed the presence of near-surface lumps of gold-bearing quartz, locally known as 'spuds', in the topmost regolith layers, which were clearly the result of denudation of outcropping auriferous quartz reefs. This, and analogies with other bedrock-alluvial gold relationships within the same drainage system would suggest that gold may have accumulated in palaeodrainage channels adjacent to the Wyalong (and Hiawatha) Goldfield. Alluvial gold was mined from small palaeochannels farther north at Billys Lookout (Bowman 1977: op. cit.; Fig. 2).

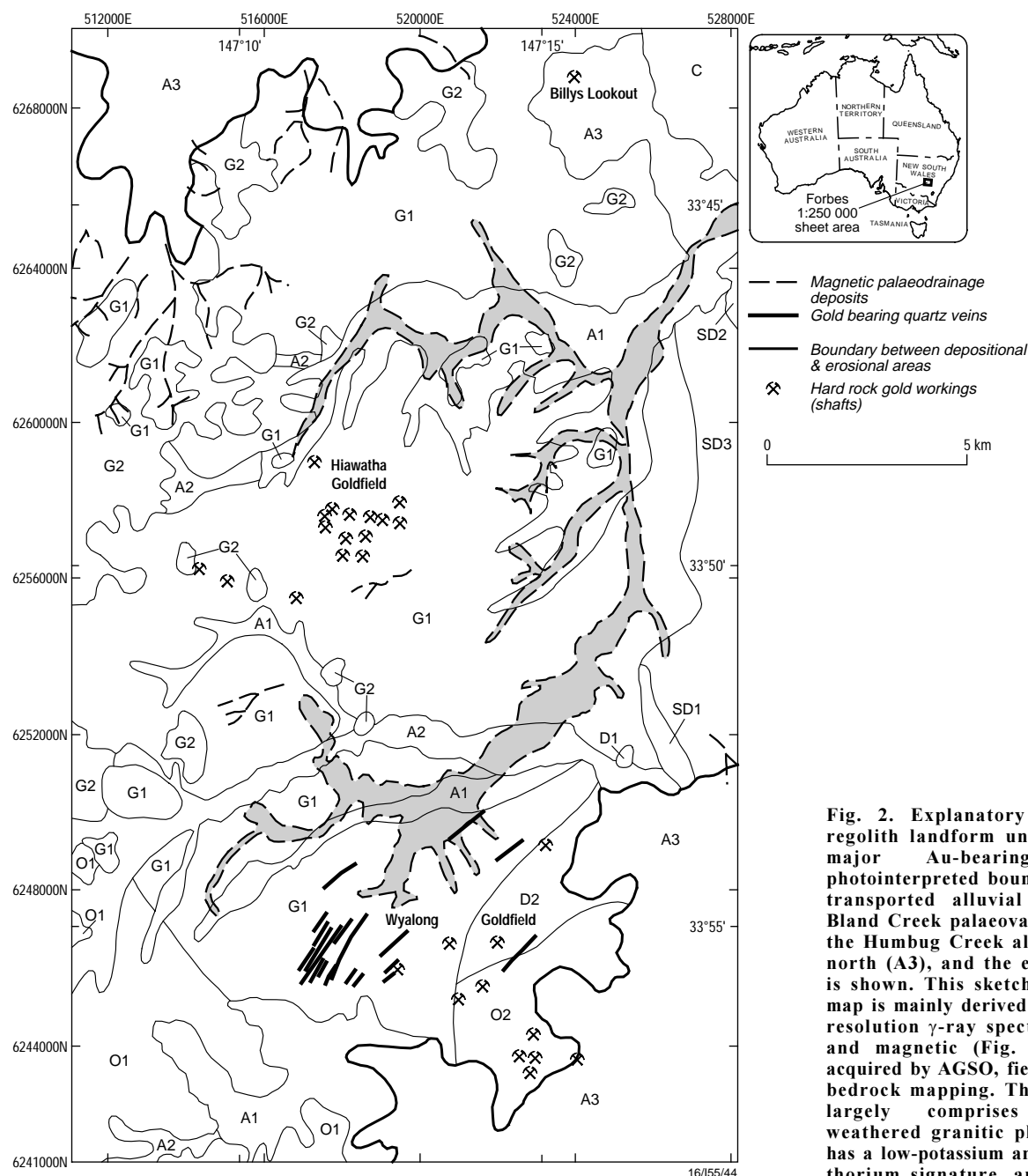
Wyalong Goldfield — primary gold characteristics

The auriferous quartz veins in the Wyalong Goldfield are structurally controlled, and localised in brittle-ductile fault zones 2.5 m wide cross-cutting the earliest Silurian Ungarie Granite (M. Duggan, AGSO, personal communication 1999). Epidote-quartz-chlorite wall-rock alteration coincides with the fault zones.

Shear-parallel veins in these fault

In this issue:

Alluvial gold potential in buried palaeochannels in the Wyalong district, Lachlan Fold Belt, New South Wales	1
Taking geology beneath cover at Broken Hill	5
Rock-property-structural-geology synergy at work in Broken Hill	7
Definition of high-temperature alteration zones with PIMA: an example from the Panorama VHMS district, central Pilbara Craton	10
Deformation and gold mineralisation of the Archaean Pilbara  Western Australia	12
Granitoid complexes and greenstone belts in the Pilbara Craton interpreted to extend down to the mid-crustal boundary at 14 km	15
Stable isotopes — signposts for mineralisation	17
Some thermal consequences of high heat production in the Australian Proterozoic	20
Interactive processing of mineral resource and occurrence data by Web users	23
Post-intrusion heating associated with high-heat-producing Proterozoic granites — implications for mineralisation?	23
The Kombolgie Subgroup — a new look at an old 'formation'	26



- A1 Alluvium/colluvium in modern valley floors; sediment derived from low-response weathered granite.
 A2 Alluvium/colluvium in modern valley floors; sediment derived from high-response Ordovician meta-sediments, and high-response weathered granite.
 A3 Thick alluvium in Bland Creek palaeochannel; variable response depending on provenance.
 C Granite-derived colluvium forming distal low-angle colluvial fan; high response.
 G1 Granite, highly weathered to 60 m-100m lag of magnetic pisoliths, veneer of residual/colluvial sediments; low-response. Erosional plains and rises.
 G2 Granite, mostly highly weathered; high-response; erosional plains and rises.
 D1 Diorite, fresh; high response; steep rise.
 D2 Diorite, weathered, masked by residual/colluvial deposits; low-response; erosional plains and rises.
 SD1 Palaeozoic strata, fresh; high total response; steep ridge.
 SD2 Palaeozoic strata, weathered outcrops on rises; high-response.
 SD3 Palaeozoic strata, weathered, veneer of residual/colluvial sediments; low-response; plains and rises.
 O1 Ordovician metasediments, slightly weathered; high-response; low ridges.
 O2 Ordovician volcanics, highly weathered; low-response; erosional plains and rises.

Fig. 2. Explanatory diagram showing regolith landform units and location of major Au-bearing reefs. The photointerpreted boundary between thick transported alluvial sediments of the Bland Creek palaeovalley to the east and the Humberg Creek alluvial plains to the north (A3), and the erosional landforms is shown. This sketch regolith-landform map is mainly derived from imaging high-resolution γ -ray spectrometric (Fig. 3A) and magnetic (Fig. 3B) data recently acquired by AGSO, field observations, and bedrock mapping. The erosional terrain largely comprises in-situ highly weathered granitic plains and rises. G1 has a low-potassium and moderate- to low-thorium signature, and is characterised by ferruginous lag derived from mottled granite. G2 has a high-potassium signature, and appears to be less weathered. Magnetically delineated palaeochannels (grey screen) containing highly magnetic detrital ferruginous pisoliths, sand, and clay cross this area, and exit to the northeast. Colluvial and alluvial deposits associated with modern drainage form a veneer across these units with two distinct provenances (A1 and A2). Variably weathered and covered diorite (D1 and D2) and sedimentary rocks (SD1–3 and O) surround the low-relief granitic landscape. In the northeast, granitic colluvium (C) is associated with steep granite hills in the northeast.

zones are much narrower (typically <1 m) and lenticular. The veins and host fault zones display a variable dip — subvertical or steeply east-dipping near the surface, and some veins flatten out at depth (<17° to the east; Watt 1899: op. cit.). Ore shoots plunge to the north in most fault zones, but to the south in the east (Markham 1987: 'Gold deposits of the Lachlan Fold Belt', NSW Geological Survey, unpublished). Steeply plunging ore shoots along strike were selectively mined. Mining extended to depths generally less than 50 m in many veins, but to 100 m in high-grade zones, and below 250 m in the Neelds and True Blue mines, where average grades were 35 and 62 g/t respectively (Aliano & Schwebel 1981: NSW Geological Survey, Report 1981/544).

Primary gold is intimately associated with pyrite. Minor sulphides include arsenopyrite, sphalerite, galena, and chalcopyrite (Watt 1899: op. cit.). Coarse gold was recovered from white quartz in veins in the east of the goldfield. Free gold is rare, but good grades were recovered by cyanidation and/or chlorination.

Oxide-zone enrichment

Gold grades of individual veins beneath the base of weathering are not uniform, but commonly <35 g/t. Despite their variability, analysis of gold production figures for individual quartz reefs shows that gold is enriched in the oxide zone (Aliano & Schwebel 1981: op. cit.), where they are typically >60 g/t. Many shafts were not deepened below the base of weathering owing to the increased difficulty of digging and diminishing grades (Watt 1899: op. cit.).

In the oxide zone, fine gold is intimately associated with iron oxides; coarse gold, with colourless, white, and reddish brown 'opaline' silica (Watt 1899: op. cit.). The base of oxidation of the host rock and quartz veins is around 50 m. Above this level, the ore and host rock could be mined with pick and shovel.

Significance of geophysical datasets for palaeochannel identification

As a contribution to the [National Geoscience Mapping Accord \(NGMA\)](#) last year, AGSO and the [New South Wales Department of Mineral Resources \(DMR\)](#) acquired high-resolution magnetic and γ -ray spectrometric datasets along lines 50 m apart 60 m above the ground in the Wyalong area. The resolution of these datasets will be compared with that of

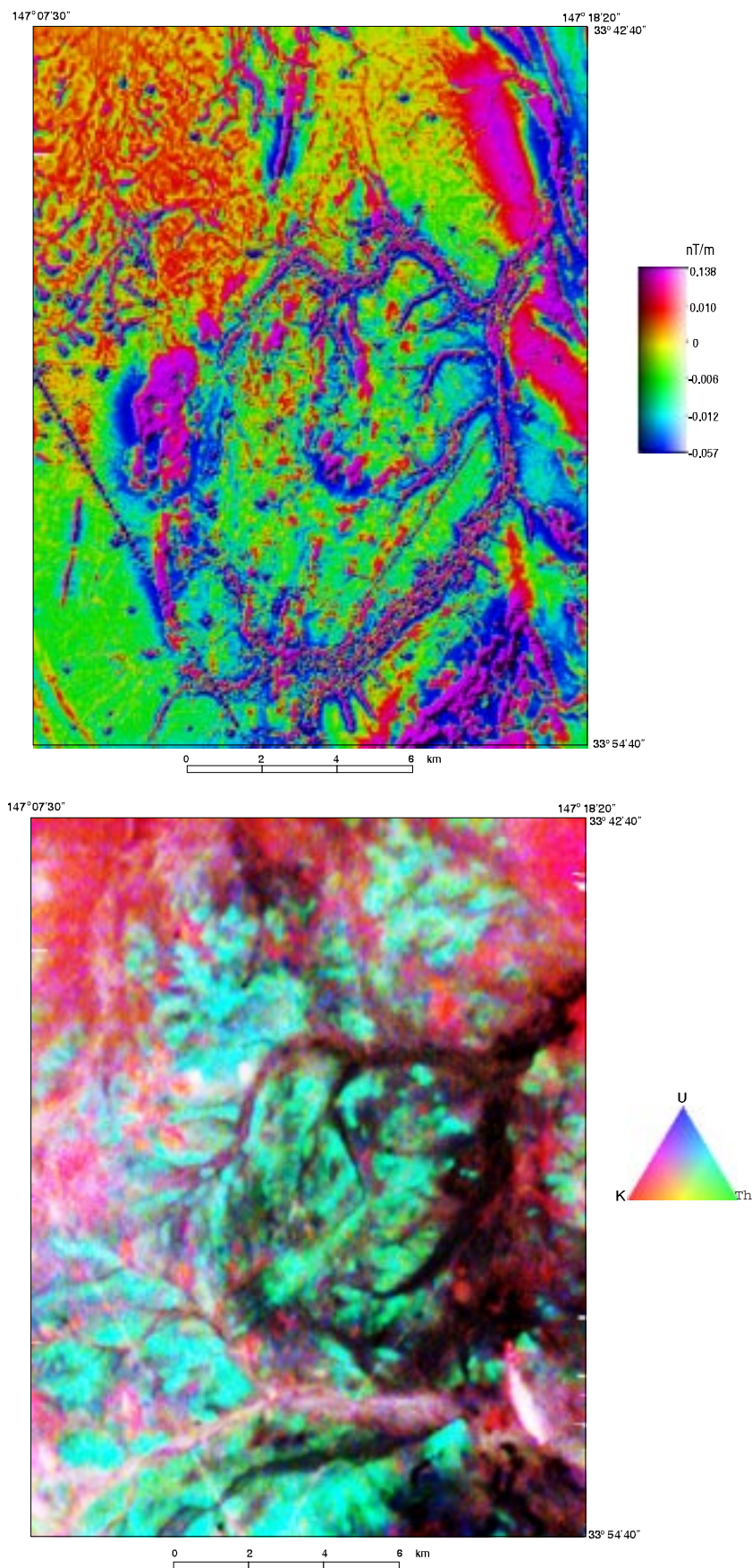


Fig. 3. High-resolution magnetic (top) and γ -ray spectrometric (bottom) images for the Wyalong district.

others acquired over the area by AGSO and exploration companies at different heights and line-spacings. The new geophysical data trace the outlines of palaeodrainage channels not previously identified (Figs. 2 and 3).

The palaeochannels in the Wyalong Goldfield are magnetically delineated, and therefore apparent in magnetic images. They are also visible on AEM images (T. Munday, [Cooperative Research Centre for Airborne Mineral Exploration Technologies](#), personal communication 1999), but not from the γ -ray data. Other magnetically delineated palaeochannels occur to the south and east. The palaeochannels contain detrital ferruginous (maghemitic) pisoliths concentrated in lenses in sand and clay (Fig. 3A). These pisoliths have high magnetic susceptibilities, which may at least in part explain the magnetic character of the palaeochannels. Palaeoflow was directed to the northeast, as indicated by the dendritic pattern in the magnetics image (Fig. 3A). The palaeochannels are not evident at the present-day land surface, but have been exposed in the West Wyalong rubbish dump. They are incised to unknown depths into weathered bedrock.

The proximity of some of the palaeochannels to the Wyalong (and Hiawatha) Goldfield — combined with the evidence for substantial surficial or near-surface mineralisation, evidence for erosion of these bedrock resources, and the juxtaposition of bedrock and alluvial deposits elsewhere in the same valley catchment — implies that they may be

prospective for alluvial gold. Further palaeogeographic reconstructive research will help identify the most prospective ones.

Preliminary comparison of data from the different geophysical datasets suggests that airborne geophysical survey lines flown 50 m apart at ≤ 60 -m elevation can reveal important information about regolith materials, including channel-fill deposits in the Bland Creek palaeovalley (T. Mackey, AGSO, personal communication 1999). However, palaeodrainage can obviously be expressed and mapped at a range of scales, and it is important to match the specifications of each geophysical survey to the scientific objectives of a study.

For our study, survey specifications facilitated the mapping of palaeochannels with a potential economic significance. In addition to their potential for hosting alluvial gold deposits, palaeochannels in the Lachlan River system are commonly reservoirs of saline groundwater (Andrews 1910: op. cit.; Wilson & McNally 1996: op. cit.). Therefore, mapping their distribution may also contribute to developing hydrogeological models for dryland salinity hazard assessment (W.R. Evans, [Bureau of Rural Sciences](#), personal communication 1999). Three-dimensional mapping of regolith materials, including palaeochannels, should also lead to a better understanding of the hydromorphic dispersion of metals.

Conclusions

Modern airborne geophysical survey

lines (magnetic and γ -ray spectrometric) flown low (60 m) and closely spaced (50 m apart) help map the distribution of buried channels in the Bland Creek palaeovalley. Owing to their proximity to bedrock gold deposits, these palaeochannels and others to the south and east of Wyalong may be prospective for alluvial gold. Similar buried palaeochannels adjacent to bedrock gold deposits in analogous settings elsewhere in the Lachlan River catchment also may be potential sources of alluvial gold.

Acknowledgments

We thank David Denham, Ian Hone, and Ken Horsfall for expediting the NGMA geophysical data acquisition, and Murray Richardson for processing the datasets; Heike Apps and Lana Murray for image preparation and figure drafting respectively; Golden Cross Resources for providing access to proprietary datasets and for discussion; and Colin Pain, Morrie Duggan, and Patrick Lyons for manuscript reviews.

¹ Minerals Division, Australian Geological Survey Organisation, GPO Box 378, Canberra, ACT 2601; tel. +61 2 6249 9847; fax +61 2 6249 9983; email ken.lawrie@agso.gov.au.

² CRC LEME (Cooperative Research Centre for Landscape Evolution and Mineral Exploration), GPO Box 378, Canberra, ACT 2601; tel. +61 2 6249 9371 (RAC), +61 2 6249 9748 (DLG); fax +61 2 6249 9983; email roslyn.chan@agso.gov.au, dave.gibson@agso.gov.au.

³ University of Canberra, Canberra, ACT 2601; tel. +61 2 6249 4097; fax +61 2 6249 9983; email nadir.kovacs@agso.gov.au.

Taking geology beneath cover at Broken Hill

Implications of structurally controlled magnetic anomalies for interpretation and mineral exploration

David W. Maidment¹, George M. Gibson¹, & John W. Giddings¹

As part of the Broken Hill Exploration Initiative, AGSO has been field-checking high-resolution aeromagnetic data acquired in 1996. This work has revealed that magnetic anomalies have multiple sources, and that many are structurally controlled and do not reflect stratigraphy.

Interpretations of aeromagnetic data in the Broken Hill region have previously assumed that magnetic anomalies were caused by magnetic stratigraphic units and hence stratigraphy could be mapped beneath cover (e.g., Tucker 1983: [AusIMM Conference](#), Broken Hill, 81–114). Some anomalies are, no doubt, stratiform (e.g., banded iron formation and specific units in the Paragon Group). Other anomalies are caused by intrusive rocks,

in particular post-peak metamorphic mafic and ultramafic rocks. However, many of the narrow linear anomalies visible on aeromagnetic images reflect magnetite development in metamorphic fabrics and structurally controlled corridors.

Structurally controlled magnetite

Early magnetite (?D₂)

The earliest magnetite formed during high-temperature metamorphism, as evidenced by sillimanite intergrowths with magnetite. In the core of the Broken Hill Synform, east of Broken Hill, magnetite–sillimanite rock causes an intense, folded magnetic anomaly (BHS, Fig. 4). The rock has a well-developed,

steeply plunging sillimanite lineation of D₂ age interpreted as a stretching lineation. A smaller magnetic anomaly, most likely caused by quartz–magnetite rock, appears to be truncated against the magnetite–sillimanite rock, which is interpreted as a shear zone.

Magnetite in S₃ fabrics

Many narrow linear anomalies parallel the trend of the S₃ regional foliation, which formed during greenschist- to amphibolite-facies metamorphism. This fabric strikes northeast in the central part of the Broken Hill Block and north-northeast in the northern part (Figs. 4 and 5).

In the Sculptures–Archery Range area, northwest of Broken Hill (SA, Fig. 4), a linear

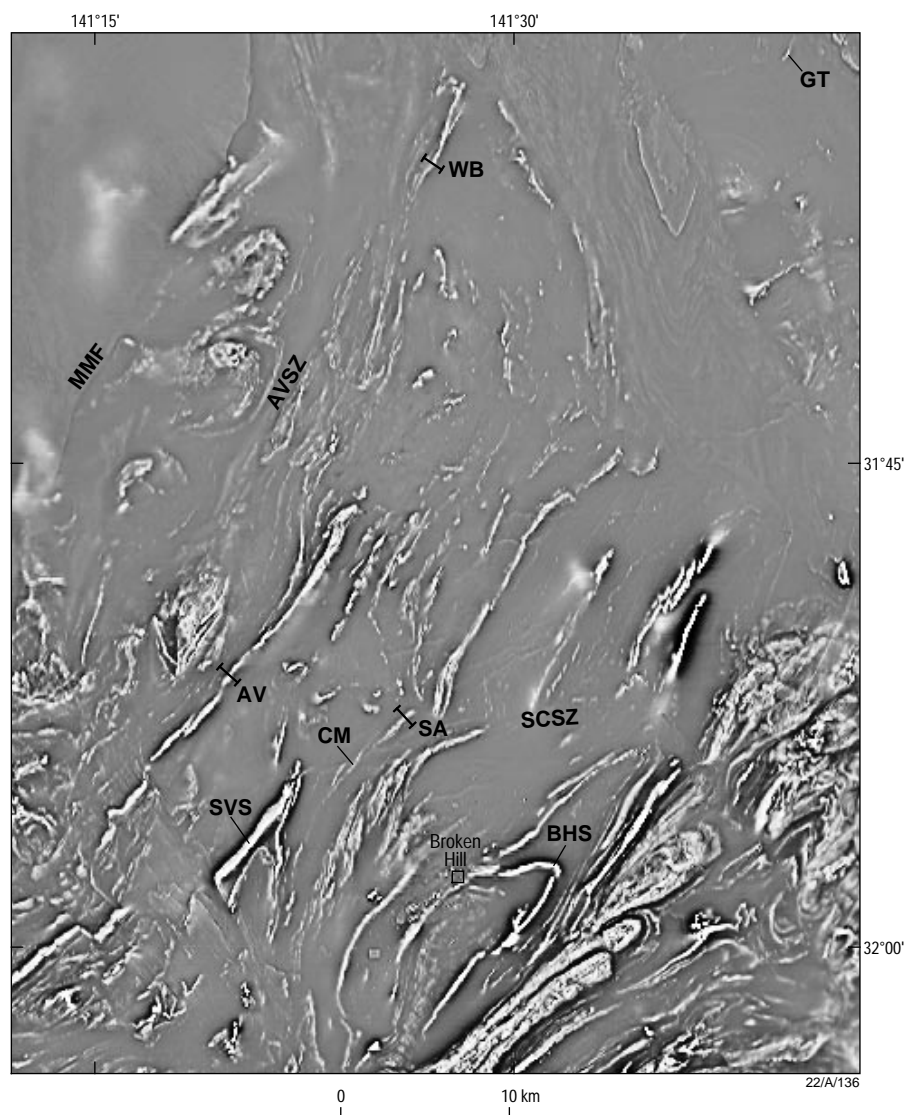


Fig. 4. First vertical derivative of total magnetic intensity for the central and northern parts of the Broken Hill Block. BHS: Broken Hill Synform; SA: Sculptures/Archery Range; WB: Waukeroo Bore; CM: Centennial Mine; GT: Gairdners Tank; SVS: Stirling Vale Synform; AV: Acacia Vale; SCSZ: Stephens Creek shear zone; MMF: Mundi Mundi Fault; AVSZ: Apollon Valley shear zone.

magnetic anomaly is sourced by pelitic and psammopelitic metasediments of the Sundown Group, in which S_3 trends northeast and is superimposed on a more gently dipping S_2 fabric. Considerable strain-partitioning accompanied the D_3 deformation; packets of more gently dipping bedding are separated by high-strain zones in which bedding, S_2 , and S_3 are steeply dipping and trend northeasterly. The magnetic anomaly in this area shares the same northeast trend and requires a steeply dipping source, suggesting S_3 controlled the distribution of magnetite. One possibility is that D_3 led to a dynamically induced increase in permeability, promoting fluid flow and the formation of magnetite. S_3 also has a strong control on magnetite distribution in the Waukeroo Bore area in the north of the block (WB, Fig. 4; see Giddings et al. this issue, pp. 7–10).

Magnetite at lithological contacts

Superposition of aeromagnetic data and geological maps reveals a close spatial association between some Potosi gneiss units and magnetic anomalies (Potosi gneiss is a local term for garnet-rich quartzofeldspathic gneiss spatially associated with Broken Hill-type mineralisation). About 1.2 km southeast of the Centennial mine, a unit of Potosi gneiss is surrounded by pelitic schist (CM, Fig. 4). The highest magnetic susceptibilities occur in metasediments adjacent to the Potosi gneiss. Both the Potosi gneiss and the metasediments away from the contact have low susceptibilities. It appears that strain has been partitioned into the contact between the moderately competent Potosi gneiss and less competent metasediments. The magnetite in this zone is interpreted to have formed during fluid flow that was focused along this contact. Similar relationships between Potosi gneiss units and

magnetic anomalies also occur west of the Parnell mine and in the Southern Cross mine area. Granite gneiss and Potosi gneiss have similar competency contrasts with surrounding metasediments, and, in some locations (e.g., Mount Darling Range), granite gneiss units also have magnetic anomalies along their margins, interpreted to be a result of the same process.

Later-stage magnetite

Although most magnetite formed at high temperatures, some also formed later at lower temperatures. An isolated magnetic anomaly near Gairdners Tank in the Euriovie Block coincides with a mapped retrograde shear zone (GT, Fig. 4). It is caused by coarse-grained euhedral magnetite in schistose metasediments, and surrounded by low-susceptibility lithologies that strike obliquely to the trend of the anomaly. The magnetite formed penecontemporaneously with a steeply dipping chlorite-rich schistosity (greenschist facies) which overprints a peak-metamorphic sillimanite-bearing assemblage.

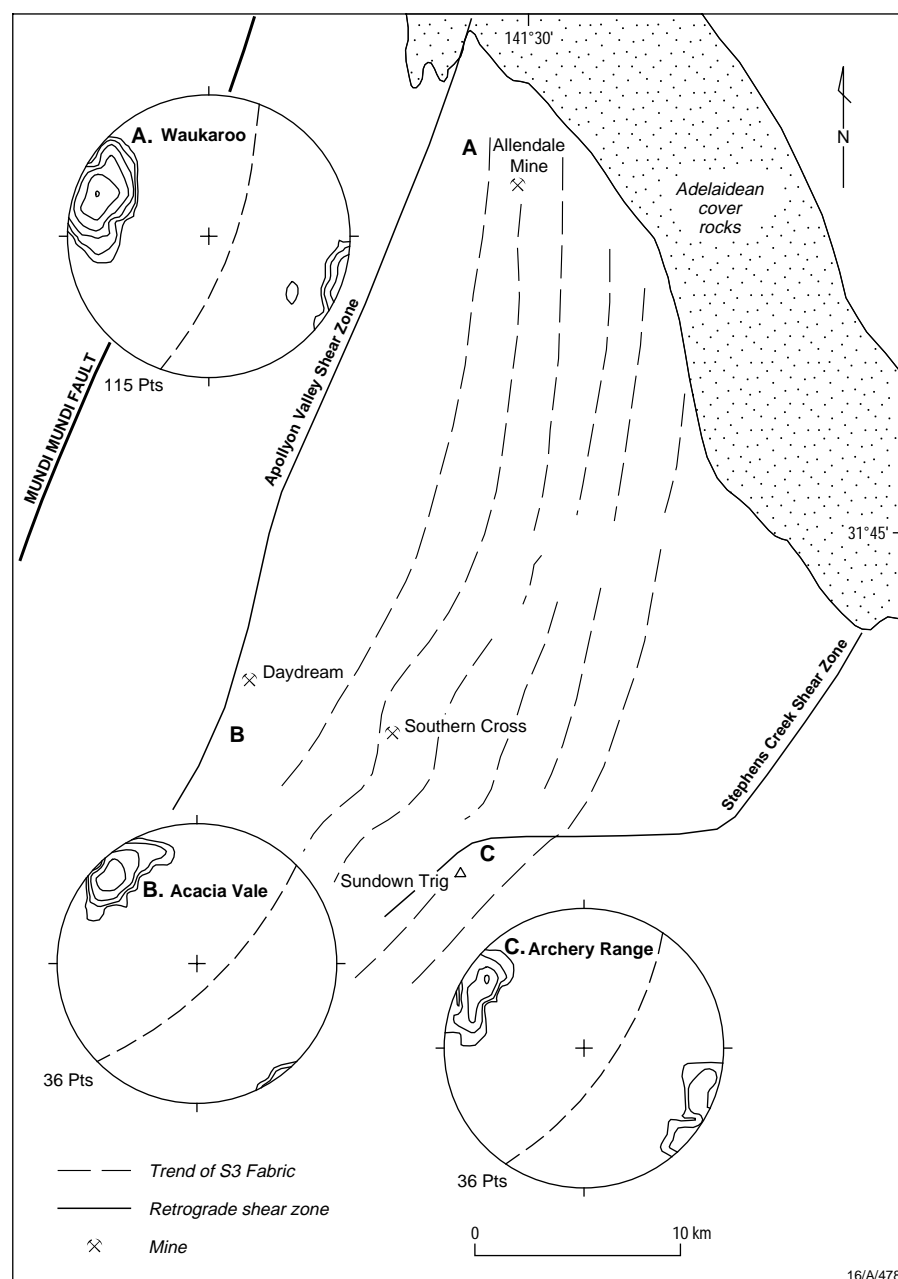
Amphibolite

Amphibolite is widely distributed in all stratigraphic units below the Sundown Group, and occurs as sills and dykes. Most amphibolite has a low magnetic susceptibility which is insufficient to produce an aeromagnetic anomaly. Some amphibolite bodies, however, have extremely high susceptibilities, and produce some of the most intense anomalies in the region (e.g., the western limb of the Stirling Vale Synform; SVS, Fig. 4). Many of these amphibolites appear to be situated close to shear zones — possibly former channels of oxidising fluids that contributed to the formation of magnetite.

Implications for interpretation and exploration

The abundance of structurally controlled magnetic anomalies in the Willyama Supergroup has important implications for aeromagnetic interpretation, irrespective of the mechanism of magnetite formation. Although some magnetic anomalies are structurally controlled, many are evidently structurally controlled, and these cannot be used to interpret stratigraphy beneath cover. Bedding and magnetic trends are not necessarily parallel, and in some locations are nearly perpendicular. Some areas are more structurally complex than aeromagnetic images suggest because the rocks were deformed before magnetite formed.

Some elements of the geology have a high susceptibility and are readily mappable from the aeromagnetic data. These include banded iron formation, some amphibolites, quartz-magnetite rocks, garnet-poor composite gneiss, and altered mafic and ultramafic intrusives. However, true stratigraphic anomalies are too sparse to readily erect a 'magnetic stratigraphy' for the Willyama Supergroup; most unaltered metasediments have a uni-



formly low susceptibility.

Structurally controlled magnetic anomalies may prove useful for delineating fluid pathways in mineral systems. Fluids that controlled the formation of magnetite may have transported base and/or precious metals. Although metal deposition may not have occurred at the time of magnetite formation, the ability to map fluid migration paths is potentially valuable for reconstructing the mineral system as a whole.

¹ Minerals Division, Australian Geological Survey Organisation, GPO Box 378, Canberra, ACT 2601; tel. +61 2 6249 9389 (DWM), +61 2 6249 9727 (GMG), +61 2 6249 9319 (JWG); fax +61 2 6249 9983; email David.Maidment@agso.gov.au, George.Gibson@agso.gov.au, John.Giddings@agso.gov.au

Fig. 5. Trend of S_3 across the central and northern parts of the Broken Hill Block (much the same area as Fig. 4). The S_3 fabric parallels many linear magnetic anomalies and suggests that S_3 had a significant regional control on magnetite formation.

Rock-property–structural-geology synergy at work in Broken Hill

A case for structural control of linear magnetic anomalies

John W. Giddings¹, George M. Gibson¹, & David W. Maidment¹

The delivery of a new generation of high-resolution aeromagnetic data for the Broken Hill Block (BHB; Haren et al. 1997: *Exploration Geophysics*, 28, 235–241) has played a significant role in helping the **Broken Hill Exploration Initiative (BHEI)** successfully achieve its brief of stimulating exploration activity (Denham et al. 1998: *AGSO Record* 1998/25, 13–16) in the region. Underpinning geological realism in interpretations of those data, however, is our understanding of what we

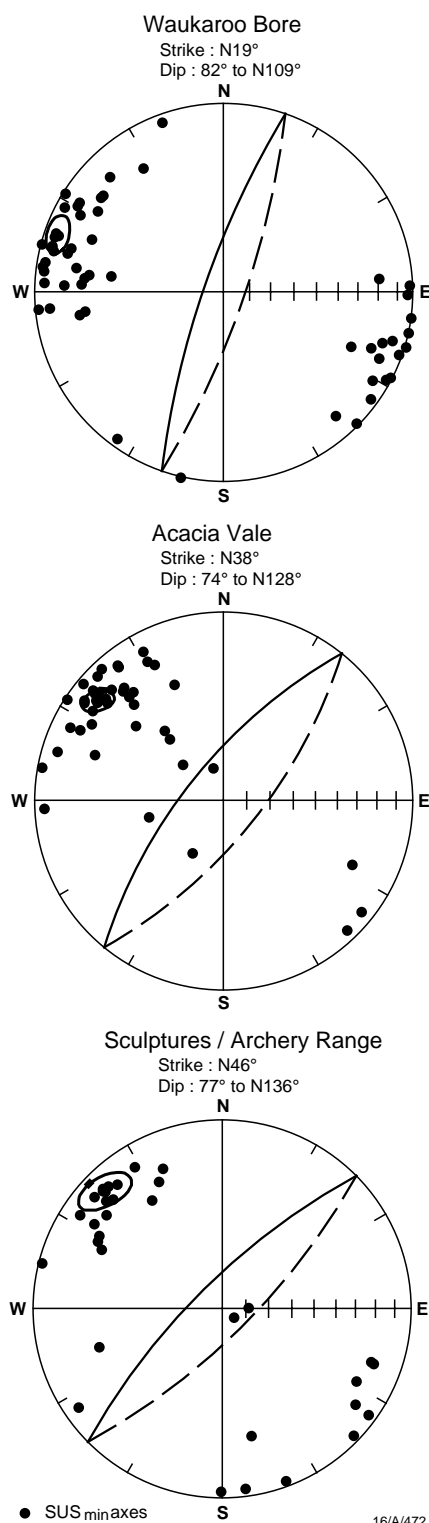
are tracing with the aeromagnetic anomalies: the more informed our understanding is, the more likely the interpretations will increase the chance of success in exploration. We present here a brief look at a combined rock-property–structural-geology study which clearly demonstrates that linear magnetic anomalies in the BHB can be structurally controlled. This outcome thus challenges the long-held view that such anomalies reflect stratigraphy, and introduces a cautionary note into

their use as markers for extrapolating lithology under cover (Maidment et al. this issue, pp. 5–7).

The linear magnetic anomalies we chose to study are part of a broad belt that sweeps across the BHB from north to southwest, and changes strike in the process from north-northeasterly to northeasterly (Fig. 4). Our more informed understanding of those anomalies and our assessment of the significance of the different parameters employed in magnetic modelling is based on combined mag-

netic field profiling, magnetic minerals determination, measurements of magnetic remanence and anisotropy of magnetic susceptibility, and detailed geological and structural mapping along traverses orthogonal to the strike of the anomalies. We targeted three anomalies, located from north to south (Fig. 4):

- north of Waukaroo Bore (WB) — trending $\sim 27^\circ\text{E}$ and hosted by the Sundown Group;
- northwest of Acacia Vale homestead (AV)



— trending $\sim 38^\circ\text{E}$ and hosted by the Thackaringa Group; and

- the Sculptures/Archery Range area (SA), northwest of Broken Hill — trending $\sim 45^\circ\text{E}$ and hosted by the Sundown Group.

Apart from the Sculptures anomaly (for which the traversing and total field measurements were conducted by the [New South Wales Department of Mineral Resources](#), a BHEI collaborator), our traverses were ~ 500 m long to ensure complete capture of anomaly profiles. Total magnetic field measurements were recorded every 5 m. Susceptibility measurements were made every 10 m, and helped locate the boundaries of the anomalous zones. Oriented cores of rock were collected along traverses for magnetic property measurements.

Magnetic properties and modelling

Using AGSO's sensitive Czech-built KLY3 Kappabridge ([Giddings & Klootwijk 1997](#); [AGSO Research Newsletter 26](#), 7–9), we identified the magnetic mineral systems in the anomalous zones from the temperature (T) variation of magnetic susceptibility (k) between -195°C and 700°C . Without exception, strongly magnetic samples yield k/T curves that indicate pure end-member magnetite in the titanomagnetite solid-solution series $\text{Fe}_{3-x}\text{Ti}_x\text{O}_4$ ($x=0$, magnetite), confirming geological evidence for magnetite as the source of these anomalies. Importantly, for the susceptibility anisotropy work, there is no indication of pyrrhotite (Fe_7S_8), an important magnetic mineral after the iron oxides but one that has a strong anisotropy related to its crystal structure.

In keeping with the ideas that certain BHB structural fabrics are magnetite-enriched, we looked at whether a relationship exists between the magnetite and petrofabric by measuring the anisotropy of magnetic susceptibility (AMS) on the KLY3 ([Giddings & Klootwijk 1997](#): op. cit.). This technique detects the presence of any preferred plane (fabric) of maximum susceptibility (the

$k_{\text{max}}-k_{\text{int}}$ axial plane, whose pole is the k_{min} axis), and for magnetite is primarily grain-shape dominated ([Borradaile & Henry 1997](#): *Earth Science Reviews*, 42, 49–93). The AMS results (Fig. 6) demonstrate that indeed a well-defined, steeply dipping magnetic fabric is present for each anomaly, and that its orientation varies between anomalies. A simple pattern emerges: southwards from WB through AV to SA, the magnetic fabric plane veers from an azimuth of 19°E and steep dip of 82° ESE (WB, anomaly trend $\sim 27^\circ\text{E}$), through 38°E and dip of 74°SE (AV, anomaly trend $\sim 38^\circ\text{E}$), to 46°E and dip of 77°SE (SA, anomaly trend $\sim 45^\circ\text{E}$). This pattern mirrors that of the structurally mapped S_3 fabric of Gibson (1999: Minfo, Department of Mineral Resources, NSW, 62, 10–12; Fig. 5), both in azimuth and dip (compare stereograms, Figs. 6 and 5). Importantly, the anomaly trends lie along the magnetic fabric trends and hence S_3 .

We investigated source body geometry by modelling the magnetic profiles in detail; our rock-property parameters provided a guide to the geological integrity of this work. The profiles, interpretations, and geological cross-sections are illustrated for the WB (Fig. 7) and AV (Fig. 8) anomalies. The shapes of the magnetic profiles indicate that each is a composite of two sources: a buried (20–50 m below the surface), steeply dipping ($\sim 80^\circ\text{ESE}$ — WB; $\sim 70^\circ\text{SE}$ — AV) tabular body (~ 125 m wide and of great depth extent) that gives the gross shape of the profile; and a number of narrower near-surface bodies that extend down to the deeper body and give high-frequency detail to the profile. These thin tabular bodies mimic the observed and marked spatial variation in surface susceptibility (up to two orders of magnitude within metres) that reflects the inhomogeneous distribution of magnetite within the anomalous zones.

Modelling with induced magnetisation alone and in conjunction with magnetic remanence enabled us to assess the importance of remanence to modelling. The initial remanence directions (freed of temporary components acquired before measurement and of lightning-struck samples) of both anomalies are moderately steep upward-pointing (normal, in the vicinity of the Earth's field) and downward-pointing (reverse), and obliquely streaked in between. We find that the reinforcement of the induced magnetisation by the normal remanence is markedly diminished in its importance by the counteracting reverse and oblique remanence, to the extent that the mean remanent field magnetisations are 4–8 times smaller than individual sample magnetisations. As a result, we find that, for these magnetite-sourced linear anomalies, remanence may be ignored in modelling the deeper tabular features, but that individual sample remanences are useful for getting the best fit to the high-frequency detail caused by the near-surface features. In fact, the difference between models (induced only and induced plus remanence) is essentially one of

Fig. 6. AMS is characterised by a susceptibility ellipsoid defined by the directions and magnitudes of the maximum (k_{max}), intermediate (k_{int}), and minimum (k_{min}) susceptibilities. This diagram shows the planes of maximum magnetic susceptibility — petrofabric planes containing the mean k_{max} and mean k_{int} axes — for the three anomalies WB, AV, and SA and mean poles (mean k_{min} axes with 95% confidence ellipses) to those planes (lower-hemisphere equal-angle projections; solid lines — traces of the planes on the upper hemisphere; dots — measurements of k_{min} axes for individual samples). Note that the planes dip steeply to ESE or SE, and veer in azimuth from ENE in the north to NE in the southern localities, showing (by comparison with Fig. 5) that the AMS is tracking the S_3 fabric.

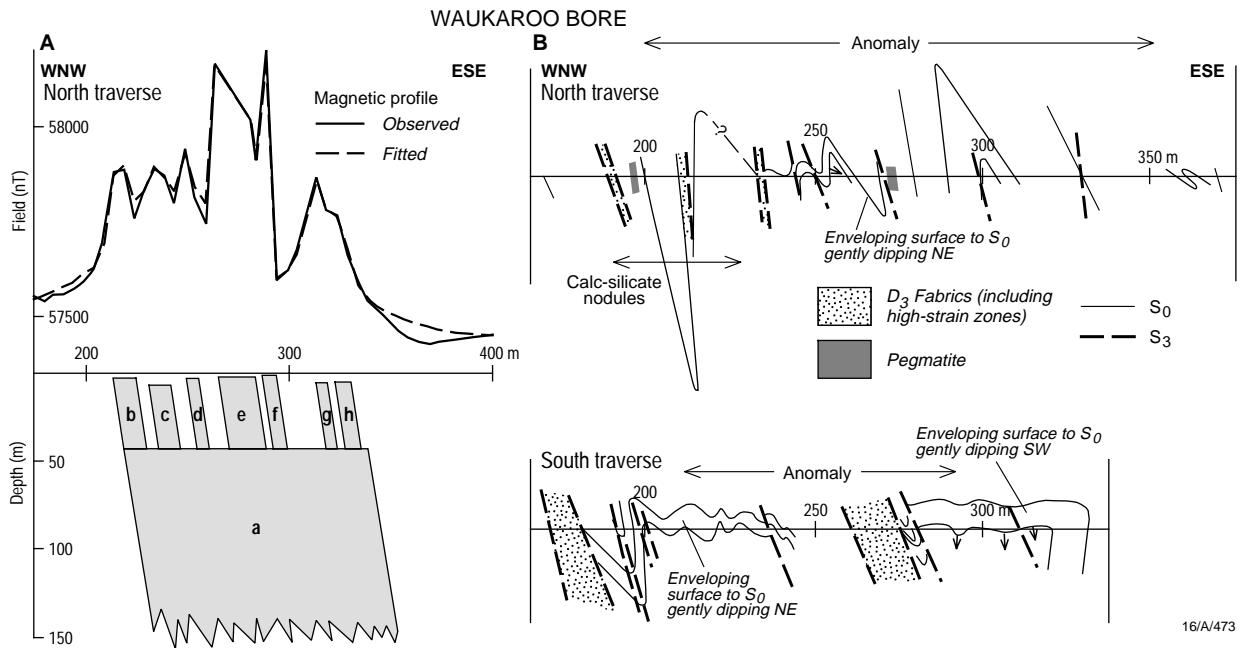


Fig. 7. Waukaroo Bore anomaly showing: (A) the anomalous part of the magnetic profile for the north traverse (two traverses were made 500 m apart along the strike of the anomaly) and, using induced and remanent magnetisation, our interpreted steeply dipping source body of great depth extent and narrower near-surface bodies (a-h represent bodies with the following susceptibilities in 10^{-5} SI — a, e, f, g: 4500; b, d: 1800; c: 3000; h: 2500 — lower values of susceptibility in the narrow near-surface bodies most likely reflect weathering); (B) the structural cross-sections for relevant parts of both the north and south traverses illustrating that the enveloping surface to bedding (S_0) is not steeply dipping but is gently dipping either to the NE or SW and that the S_3 fabric dips steeply to the ESE like our modelled source geometry. We have a clear case of structural rather than stratigraphic control of this anomaly.

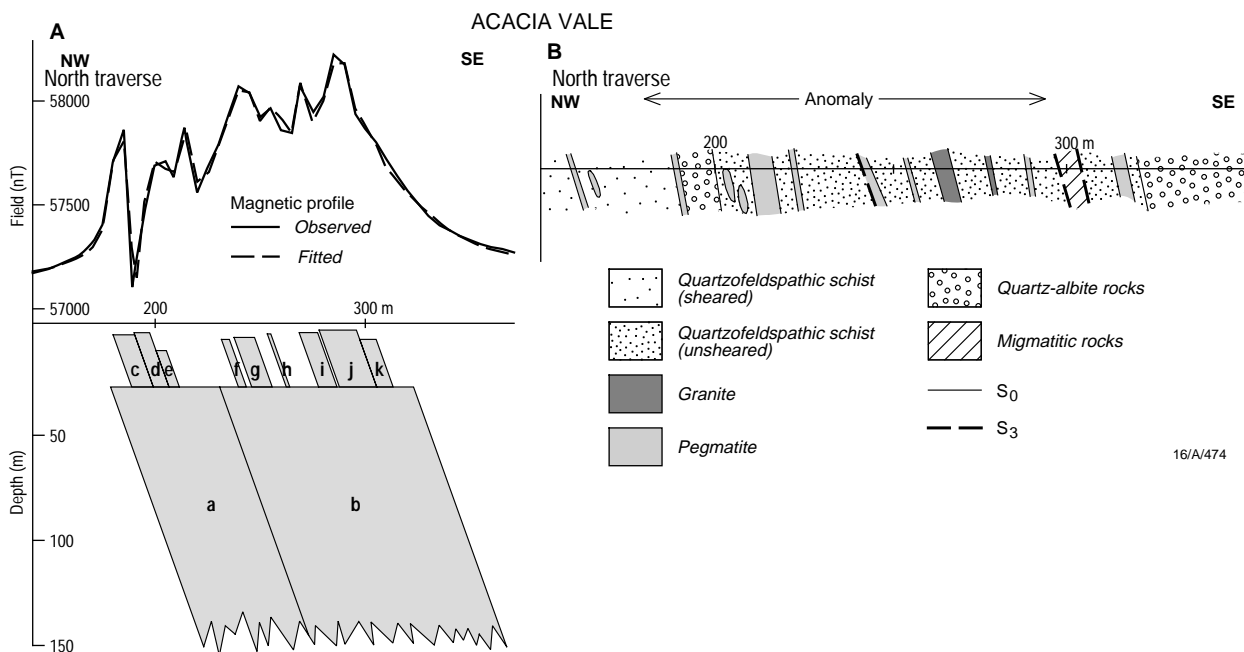


Fig. 8. Acacia Vale anomaly showing: (A) as in Fig. 8a, our interpreted source geometry for the north traverse magnetic profile (susceptibilities in 10^{-5} SI for a-k — a,k: 2000; b: 5000; c: 1100; d: 2500; e: 4800; f,i: 1200; g: 1700; h: 1900; j: 3200; the lower susceptibility for part of the deep body, a, is consistent with geological evidence for magnetite depletion in this zone owing to bleeding of magnetite into the reactivated fabric of the adjacent retrograde shear zone); (B) structural cross-section for the traverse illustrating that bedding (S_0) and S_3 have similar steep dips, so that the case for structural control can be challenged on the basis that S_3 could have inherited a pre-existing magnetite-rich S_0 fabric (stratigraphic control).

repositioning the less important near-surface bodies to realign the computed profile for the effect of remanence: the shape and dip of the main tabular bodies remain unchanged.

Structural control of anomalies by S_3

How do the models fit with the mapping and AMS data? We note that the dip and dip sense required of the tabular bodies by the shape of the anomaly profiles (Figs. 7, 8) are consistent with the dip and dip sense of the magnetic fabrics measured for the anomalous zones (Fig. 6) and that those fabrics are the S_3 fabric (Fig. 5). Hence the tabular bodies must represent the magnetite-rich S_3 fabric.

For WB, the geological cross-sections (Fig. 7) show that the enveloping surface to S_0 (bedding) dips gently to the NE and SW.

However, we demonstrated that the anomalous zone here dips $\sim 80^\circ$ ESE and is the magnetite-rich S_3 fabric. Clearly, this is a case of an anomaly controlled by structure, not stratigraphy: magnetite-impregnation of S_3 was probably associated with circulating fluids. Results (not illustrated) indicate a similar origin for the SA anomaly. For AV (Fig. 8), the interpretation is equivocal: S_0 and S_3 have similar steep dips so the case for structural control can be challenged on the basis that S_3 could have inherited a pre-existing magnetite-rich S_0 fabric (bedding — stratigraphic control).

Irrespective of the control mechanism for the AV anomaly, we have added another cautionary note to others concerning the use of linear anomalies for mapping geology in concealed areas: although some undoubtedly re-

flect lithology, others will certainly reflect structure. Recognition of structurally controlled anomalies and the implications stemming from their association with fluid movement adds an important dimension to exploration strategies.

Acknowledgments

We thank Tony Meixner and Peter Gunn for introducing us to the intricacies of magnetic modelling; and Alan Whitaker and Chris Klootwijk for reviewing the manuscript.

¹ Minerals Division, Australian Geological Survey Organisation, GPO Box 378, Canberra, ACT 2601; tel. +61 2 6249 9319 (JWG), +61 2 6249 9727 (GMG), +61 2 6249 9389 (DWM); fax +61 2 6249 9983; email John.Giddings@agso.gov.au, George.Gibson@agso.gov.au, David.Maidment@agso.gov.au

Definition of high-temperature alteration zones with PIMA: an example from the Panorama VHMS district, central Pilbara Craton

David L. Huston¹, Julianne Kamprad¹, & Carl Brauhart²

The Panorama volcanic-hosted massive sulphide (VHMS) district in the central Pilbara is an ideal natural laboratory to test newly developed exploration techniques, as it is perhaps the best exposed, least deformed district of its type in the world. Our studies there show that PIMA (portable infrared mineral analyser) analysis effectively defines local-scale alteration zones, and complements alteration mapping as an exploration tool. The depth ratio of Al—OH to Fe—OH absorption features in PIMA spectra corresponds to sericite—chlorite ratios, and effectively maps alteration facies.

The Sulphur Springs deposit is the largest of several VHMS deposits that occur at or near the top of the 3.24-Ga Kangaroo Caves Formation in the Panorama district. The Kangaroo Caves Formation consists of andesitic to rhyolitic volcanic rocks, and has been intruded by the polyphase, subvolcanic Strelley Granite (Fig. 9a). The granitic and volcanic rocks are overprinted by three main alteration assemblages in the Sulphur Springs area (Fig. 9b):

- chlorite—quartz—albite \pm carbonate \pm pyrite, the regional background alteration assemblage;
- chlorite—quartz, which forms a pipe-like zone below the deposit and a semi-conformable zone at the base of the andesite; and
- feldspar—sericite—quartz, which occurs mainly in dacite lateral to the de-

posit (Brauhart et al. 1998: Economic Geology, 93, 292–303).

Methodology

The PIMA is a spectrometer that measures the infrared (1300–2500-nm wavelength) radiation reflected from illuminated geological samples. Light interacting with the molecular bonds of a sample is absorbed at wavelengths that characterise the sample and causes a spectral response. These characteristic absorption features can be used to identify minerals, particularly hydrous minerals commonly formed during hydrothermal alteration.

PIMA spectra (e.g., Fig. 10) were collected from 63 fresh-rock powders from the Sulphur Springs area that were also analysed for oxygen isotopes (Huston et al. 1998: AGSO Research Newsletter, 29, 14–16) and whole-rock geochemistry. Before they were interpreted, the raw spectra were transformed to remove curvatures caused by major absorption features outside the spectral range of interest (e.g., a hull transformation). The resulting spectra were then classified by shape into spectral groups, and the depth and position of the peak within the Al—OH (2180–2220 nm) and Fe—OH (2230–2295 nm) absorbance bands were measured for each spectrum.

Results

Qualitative examination indicates that most spectra are dominated by chlorite

and/or sericite. The spectrum of one diorite sample indicated the presence of actinolite—tremolite, and several spectra indicated the presence of minor kaolinite.

The PIMA spectra did not detect carbonate minerals, even though background-altered andesite contains significant ankerite/calcite. This apparent inconsistency results from the requirement for a high abundance of carbonate minerals before PIMA will detect them. The PIMA spectra do not indicate the presence of other hydrous minerals in the samples analysed. All the spectra and a more detailed analysis of the results are presented in Huston et al. (1997: AGSO Record 1997/14).

The depth (D) of a peak in the Fe—OH and Al—OH absorbance bands for each sample may be expressed as a ratio ($D_{[2230-2295]}/D_{[2180-2220]}$), which approximates closely the chlorite/sericite ratio (e.g., Huston et al. 1997: op. cit.). According to the spatial variation of this ratio (Fig. 9c), high $D_{[2230-2295]}/D_{[2180-2220]}$ values (>0.5) correspond broadly to the chlorite—quartz alteration zone (Fig. 9b). The highest values (>2.0) occur in the andesite directly below the Sulphur Springs gossan and extend west to a major dolerite dyke. A smaller, stratiform zone of high values (>2.0) corresponds to the southeastern extension of the chlorite—quartz alteration zone at the base of the andesite. PIMA analysis also indicates the presence of a 300–400 m wide, stratiform zone with

higher $D_{[2230-2295]}/D_{[2180-2220]}$ values (0.5–2.0) in the upper part of the background alteration zone southeast of the chlorite-quartz pipe; field mapping has not revealed a corresponding change in

alteration mineralogy in this region. Low $D_{[2230-2295]}/D_{[2180-2220]}$ values (<0.5 ; generally 0.0) are restricted to sericite-dominant alteration zones, to the granite and mafic intrusive complex, and to the lower part

of background-altered andesite. Whereas most changes in $D_{[2230-2295]}/D_{[2180-2220]}$ are sharp, those between sericite-altered dacite and the upper part of background-altered andesite are gradational.

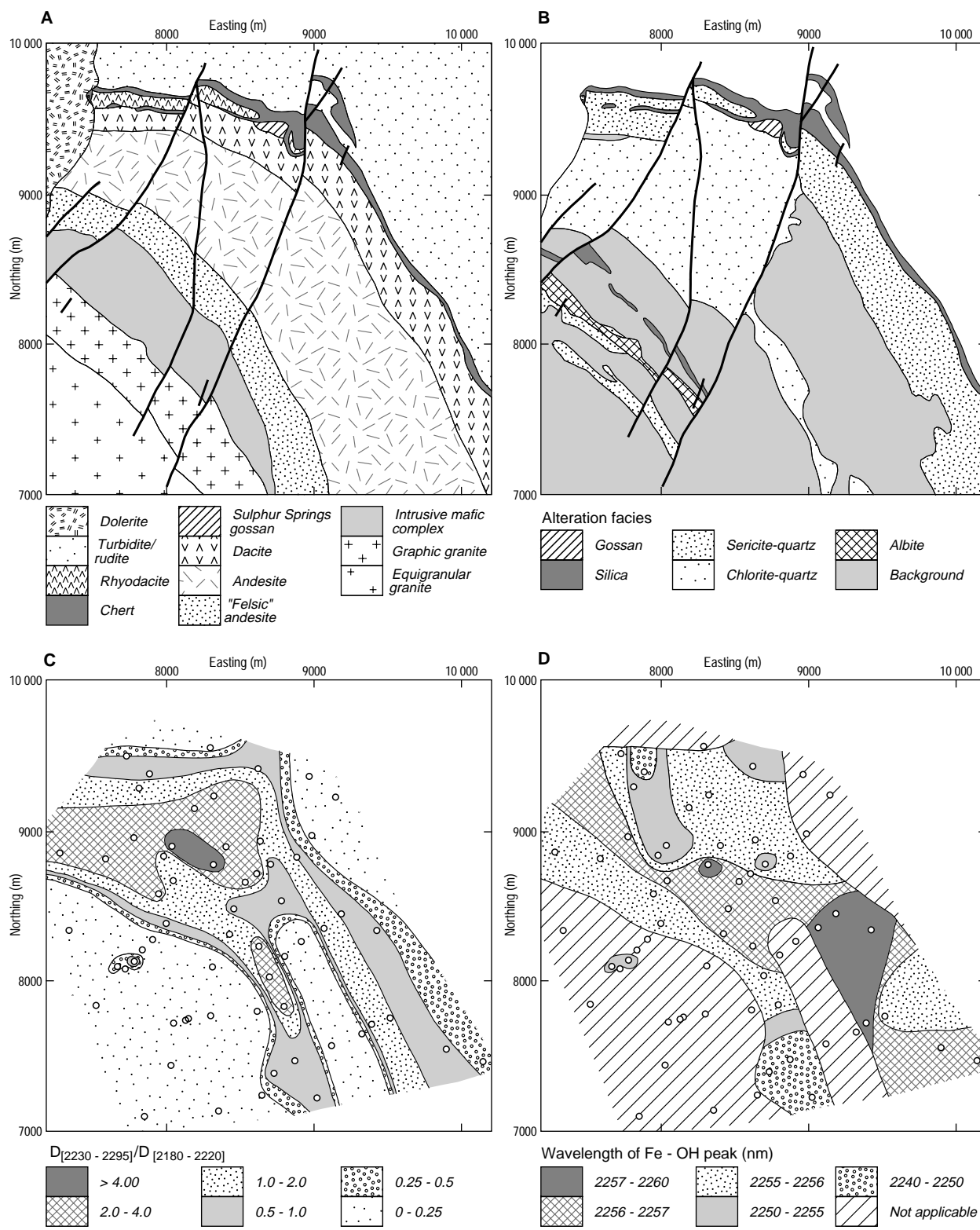


Fig. 9. Plans of the Sulphur Springs area showing: (a) geology, (b) alteration assemblages, (c) variation in the depth ratio of the Fe-OH to Al-OH absorption features, and (d) variations in the wavelength of the Fe-OH absorption feature. Open circles represent sample locations.

Variations in the wavelength of the Fe–OH and the Mg–OH absorption bands can be used as a qualitative indication of chlorite composition. In this study, we used the Fe–OH absorption band (2240–2260 nm; Fig. 9d) because the Mg–OH absorption band (2320–2360 nm) was poorly defined for many samples. Low-wavelength values indicate Mg-rich chlorite, whereas higher values indicate Fe-rich chlorite (Pontual et al. 1997: 'Spectral analysis guides for mineral exploration', 7). Most Fe–OH absorbance peaks around Sulphur Springs are between 2255 and 2257 nm, which indicates Fe-rich chlorite. Values below 2255 nm are restricted to the northwestern part and the southeasternmost extension of the chlorite–quartz alteration zone. Values greater than 2257 nm are restricted to a small part of background-altered andesite with high $D_{[2230-2295]}/D_{[2180-2220]}$.

Exploration applications and further work

The PIMA parameters discussed are potentially useful as vectors in semiregional to deposit-scale exploration. The most effective parameter is $D_{[2230-2295]}/D_{[2180-2220]}$, which is a measure of the chlorite/sericite ratio. Variations in relative chlorite and sericite abundances are common in many VHMS districts, in which chlorite generally is enriched in alteration zones proximal to deposits whereas sericite is enriched distal to deposits (cf. Franklin et al. 1981: *Economic Geology*, 75th Anniversary Volume, 485–627). The PIMA results at Sulphur Springs are consistent

with this generalisation. This zonation occurs over a distance of a kilometre or more, which suggests that this ratio can be used as a semiregional exploration guide. However, variations in the wavelength of the Fe–OH peak, which reflect systematic compositional variations, are not as useful.

The results presented here also have implications for hyperspectral remote sensing as a tool for defining exploration vectors at the regional scale in well-exposed terrains. AGSO is presently a contributor to a project (funded by MERIWA, the Minerals & Energy Research Institute of Western Australia, and operated by CSIRO) designed to assess

the applicability of the hyperspectral HYMAP remote-sensing method to mineral and alteration mapping in the Panorama VHMS district.

Acknowledgments

This contribution benefited from reviews by Terry Mernagh and Alastair Stewart.

¹ Minerals Division, Australian Geological Survey Organisation, GPO Box 378, Canberra, ACT 2601; tel. +61 2 6249 9577 (DLH), +61 2 6249 9274 (JK); fax +61 2 6249 9983; email David.Huston@agso.gov.au, Julie.Kamprad@agso.gov.au

² Centre for Strategic Minerals, University of Western Australia, Nedlands, WA 6009; tel. +61 8 9380 1871; fax +61 8 9380 1178; email cbrauhar@geol.uwa.edu.au

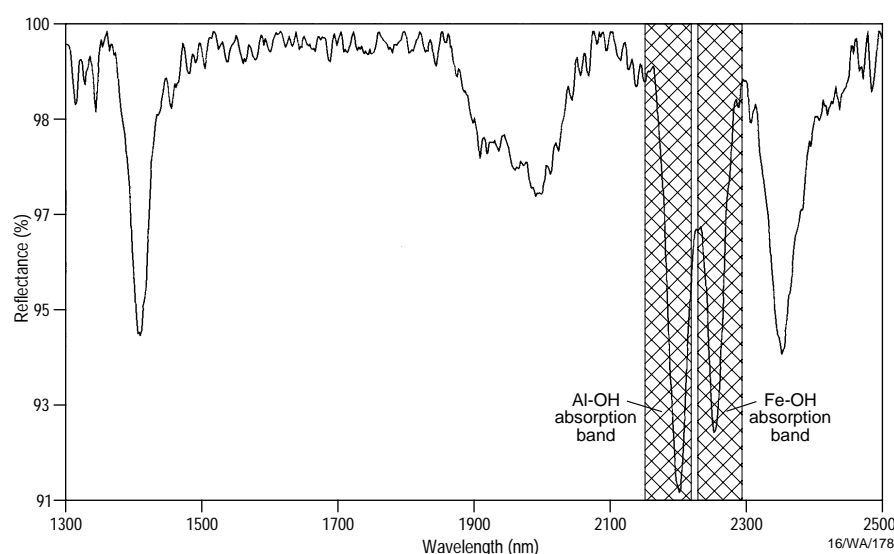


Fig. 10. PIMA spectrum for sample 207497 showing the Al–OH and Fe–OH absorption bands (cross-hatched areas). This sample has a $D_{[2230-2295]}/D_{[2180-2220]}$ of 0.87.

Deformation and gold mineralisation of the Archaean Pilbara Craton, Western Australia

Richard Blewett¹ & David L. Huston¹

Early to late Archaean (3600–2780 Ma) lithostratigraphy and structures in the north Pilbara granite–greenstone terrain are so well preserved over wide areas, despite locally intense deformation, that we can link the chronology of crustal/craton-scale events to episodes of mineralisation. Mineralising events coincided with the formation, deformation, and stabilisation of the Pilbara craton over its 800-Ma evolution, and with the subsequent initiation of the Hamersley Basin (~2780–2400 Ma). As a contribution to the joint AGSO–GSWA (Geological Survey of Western Australia) 'North Pilbara' project for the National

Geoscience Mapping Accord, we discuss the tectonothermal and related mineralising events of the north Pilbara granite–greenstone terrain (Fig. 11).

Geological framework

Lithostratigraphic mapping in the north Pilbara granite–greenstone terrain distinguishes up to nine greenstone (volcanic–sedimentary) packages and at least 10 largely coeval felsic intrusive events (e.g., Hickman 1983: GSWA Bulletin 127; Krapez 1993: Precambrian Research, 60, 1–45; Fig. 12). Recent lithostratigraphic and geochronological studies have revealed substantial differences between the east-

ern and western parts of the terrain (Hickman 1997: GSWA Annual Review, 76–81).

In the eastern, older part of the craton, younger granitoid phases tended to be intruded into older granitoid rocks (although not exclusively), forming large (100+ km diameter) granitoid complexes. Contemporaneous greenstones accumulated episodically in synforms between the developing granitoid complexes, most across unconformable contacts (e.g., Buick et al. 1995: *Nature*, 375, 574–577; Van Kranendonk 1998: GSWA Annual Review 1997–98, 63–70). These observations have led some workers to suggest that

crustal overturning and/or passive gravity-driven tectonics was the driving force behind the crustal evolution of the east Pilbara (Hickman 1997: op. cit.; Collins et al. 1998: *Journal of Structural Geology*, 20, 1405–1424).

In the west Pilbara, two distinct greenstone packages — the 3270-Ma Roebourne Group and 3120-Ma Whundo Group — occur on either side of the Sholl shear zone, a multiphase strike-slip fault (Smithies et al. 1999: *Precambrian Research*, 94, 11–28). Locating a boundary or suture between the east and the west Pilbara is a continuing problem. This search is frustrated by deep crustal

boundaries interpreted from gravity and magnetic data not corresponding to faults at the surface.

We have established an event chronology based on macro- and mesoscale structural observations (new work and published compilations; details at <http://www.agso.gov.au/minerals/pilbara/table.html>). In it, we identify eight phases of penetrative deformation manifested by such features as folds, schistosity, and shear zones (Fig. 12), and thus extend the fourfold division of Hickman (1983: op. cit.). What caused the deformation? A number of models have been proposed, including:

- intraplate (extensional and compressional) tectonism with changes in far-field horizontal stresses controlling the system;
- subduction-related marginal processes and accretion similar to those operating during the Phanerozoic; and
- diapirism and partial crustal overturn caused by density contrasts between the granitoids and greenstones.

Instead of one single mechanism, all these processes may have been involved in shaping the Pilbara over the 800 Ma of its development. Such interpretations have an impact on metallogenic models

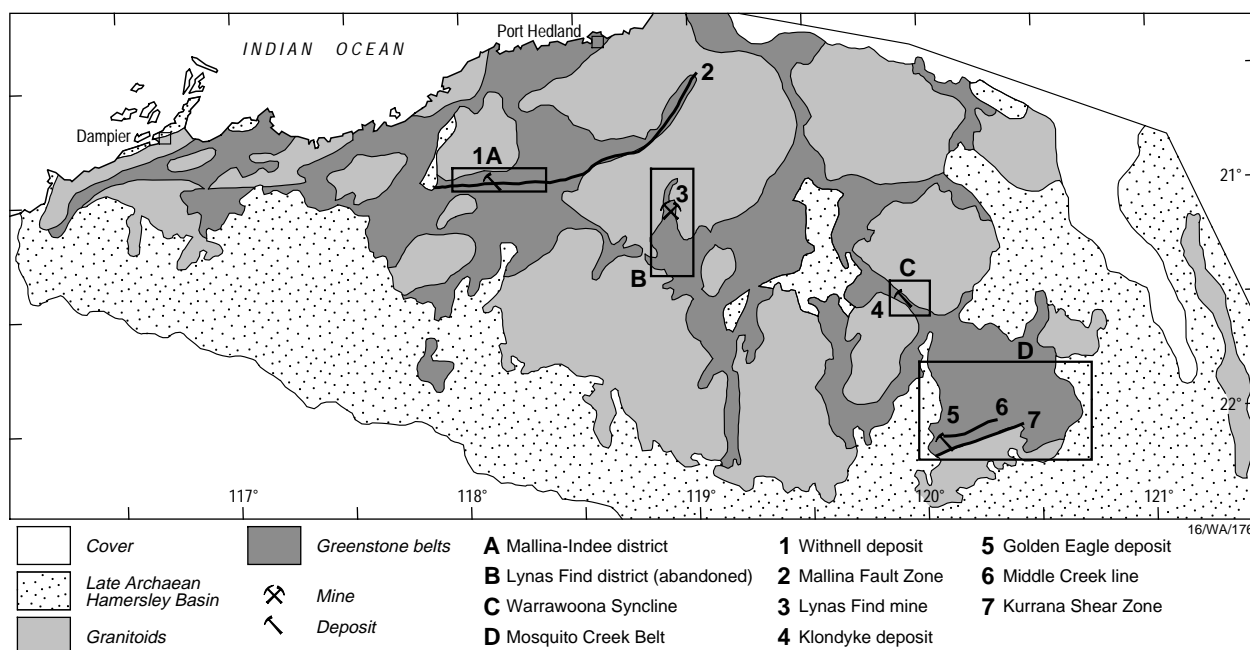


Fig. 11. North Pilbara Craton generalised geology, and localities discussed in the text.

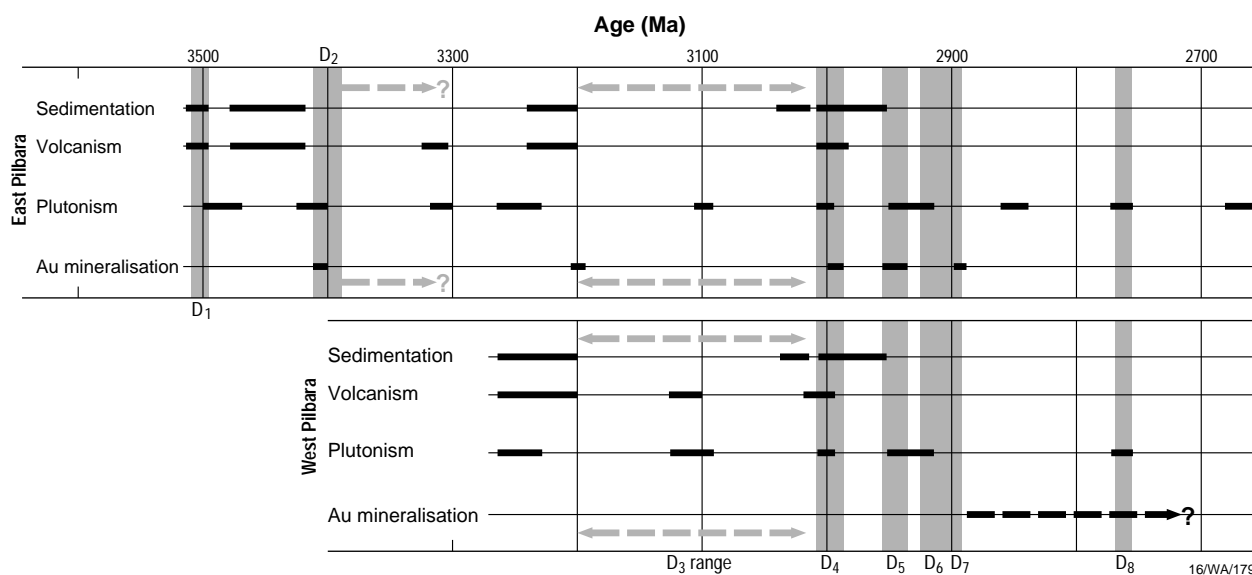


Fig. 12. Pilbara Craton event chart, showing correlative penetrative deformational, plutonic, volcanic, and mineralising events from 3500–<2700 Ma.

Table 1. Host and structural and age parameters of gold mineralisation at selected locations in the Pilbara Craton

<i>District/deposit</i>	<i>Host rocks</i>	<i>Structural controls</i>	<i>Structural level</i>	<i>Absolute age (Ma)</i>	<i>Structural age</i>
Bamboo Creek	Komatiite, Warrawoona Group	E–W-trending mylonitic shear zones (sinistral NE up shear)	Moderate to deep	3410	Syn-D ₂
North Pole/Normay	Mafic schist, Talga Talga Subgroup	E–W-striking, N-dipping veins		3405	Syn-D ₂
Warrawoona/Klondyke	Mafic and ultramafic schists, Warrawoona Group	Subvertical lineation caused by intersection of S ₂ ? and S ₅ ?	Moderate to deep	3400	Syn-D ₂
Lalla Rookh/Lalla Rookh	Basalts, basal part of Salgash Subgroup	Dilational zones in axial regions of E–W-oriented ‘kink’ folds	Moderate?	3200	Syn-D ₃ ?
North Shaw/Big Bertha	Metabasalts, Warrawoona Group	Moderately east-dipping veins		2990	D ₄ ?
Nullagine/Golden Eagle	Turbidites, Mosquito Creek Group	Upright limb of reclined, south-verging F4 fold	Moderate to deep	2905?	Syn-D ₄ or -D ₅ (3000–2950 Ma)
Lynas Find	Amphibolite and talc schist, Warrawoona Group	Highly sheared contact (thrust?) between amphibolite and ultramafic schist		2890	Syn- or post-D ₄
Indee–Withnell	Turbidites, Mallina Formation	Tension-gash array developed on E–W normal faults (S side up)	Moderate	?	Post-D ₇ (<2880 Ma)
Indee–Peawah	Turbidites, Mallina Formation	Tension-gash array developed on E–W normal faults (S-side up)	Moderate	?	Post-D ₇ (<2880 Ma)
Indee–Becher	Turbidites, Mallina Formation	N–S veins	Shallow	?	Post-D ₇ (<2880 Ma)

in terms of linking deposits in time and space (e.g., far-field or marginal tectonic forces) rather than them being random, isolated occurrences (diapirism).

Implications for gold mineralisation

Gold mineralisation was episodic in the Pilbara, in concert with magmatism and deformational events (Fig. 12). Lead-isotope data suggest that epigenetic gold deposits formed at ~3410 Ma (D₂), ~3200 Ma (D₃), ~2990 Ma (D₄), and ~2900 Ma (D₇), and structural relations suggest further events at <3000 Ma (D₄ or D₅) and <2880 Ma (D₈; Fig. 12, Table 1). Although these structural and absolute-age data constrain gold mineralisation temporally, they need the support of information that discriminates the structural controls on mineralisation before we can effectively explore for deposits and understand the mineral systems. These controls are

summarised for a number of deposits in Table 1.

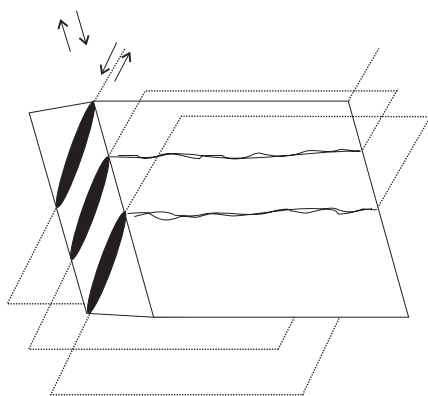
The host rocks, structural controls, and structural levels of gold mineralisation in the Pilbara are varied (Table 1). Most deposits, including the largest ones, are hosted by either mafic to ultramafic volcanics of the Warrawoona Group or turbidites of the Mallina Formation or Mosquito Creek Group.

Many of the gold deposits are associated with shear zones and the faulted contacts between units of contrasting competencies and lithologies. These shear zones and faults vary in strike length, throw, geometry, and structural level now exposed. The important control of tensional zones in regional faults is illustrated at the Withnell deposit, one of the important new gold prospects along the Mallina Fault Zone (Smithies 1998: Yule 1:100 000 geological map, GSWA) in the Mallina–Indee district

(Fig. 11). Analysis of the regional structure, coupled with mapping and logging drillcore, indicate that gold mineralisation postdated D₇, and formed under a moderate- to high-level structural (e.g., brittle) and fluid regime. The deposit appears to be hosted in a tension-gash array developed during normal faulting with downthrow to the north (Fig. 13A).

Sheared contacts between units with a marked competency contrast controlled mineralisation in the Lynas Find district (Fig. 11), where the sheared (D₄) contacts between ultramafic rocks and highly altered mafic schists typically host gold deposits. As some of the shear zones have displacement indicators of high-angle reverse-faulting, blind (stacked) orebodies may have developed in the footwalls of thrust-planes (Fig. 13B).

A pervasive subvertical lineation formed by the intersection of two orthogonal foliations (S₂ and S₅?) is promi-



nent in the complex geology of the Klondyke district in the Warrawoona Syncline (Figs. 11 and 13C). Boudinaged and sheared sulphide-bearing veins (S_2 ?) developed with long axes plunging gently in a steeply dipping fabric. Other boudin axes plunge steeply. Vearncombe (1995: Report to CRA Exploration, p. 45) identifies four phases of deformation; the main schistosity was associated with mineralisation and S-directed thrusting. An alternative view (Collins et al. 1998: op. cit.) is that the deformation is a function of partial crustal overturning and granitoid diapirism.

At Golden Eagle, in the Mosquito Creek Belt (Fig. 11), gold is stratabound in the upward-facing limb of a reclined anticline (F_4) that plunges subhorizontally to the east (Fig. 13D). The timing of mineralisation is unknown, but this 'favourable' structure continues eastwards with a shallow plunge. Shear zones and high-strain zones (D_5) control the Middle Creek line (Fig. 11). Their late dextral (D_5) kinematics is consistent with movement on the regional Kurrana Shear Zone, which marks the southern margin of the belt.

Study of these individual districts demonstrates the variability and importance of structural control on gold mineralisation in the Pilbara. Moreover, it indicates that, unlike the temporally con-

strained Yilgarn gold events (see Yeats & McNaughton 1997: AGSO Record 1997/41, 125–130), gold mineralisation developed at many periods in the evolution of the Pilbara Craton. In addition, much of the mineralisation appears to have been syntectonic rather than post-tectonic. An understanding of these structural and temporal controls on mineralisation is essential for gold exploration in the Pilbara.

Conclusions

- Regional structural analysis combined with district- and deposit-scale studies have improved our understanding of the Pilbara gold mineral systems. Further detailed and regional studies are clearly needed.
- The recognition of late (e.g., post- D_7) high-level gold associated with normal faults has implications for greater Pilbara prospectivity, especially close (in time and structural level) to the Hamersley unconformity.
- There is currently little consensus on the tectonic evolution of the Pilbara Craton, for which models including intraplate, marginal/subduction, and diapirism have been proposed. It is possible that all three mechanisms have occurred at some time in the craton's long history.

Acknowledgments

We thank Arthur Hickman, Martin Van Kranendonk, and Hugh Smithies (GSWA) and Kevin Cassidy, David Champion, and Shen-su Sun (AGSO) for their constructive reviews, and acknowledge that they may not necessarily agree with all the statements in this paper

Fig. 13. (A, top) Stylised diagram of tension-gash veins developed in a competent unit with bedding-parallel faulting (viewed north), where σ_1 is vertical (normal Andersonian faulting). Vein tips intersect the surface and strike east-west. The geometry predicts 'stacked' veins, each of which has a limited vertical extent. (B, upper middle) Sheared altered ore zone in McPhees pit in the Lynas Find district (viewed southeast). (C, lower middle) Intense intersection lineation at the Klondyke deposit (viewed southeast). (D, bottom) Reclined parasitic F_4 fold in the centre of the Golden Eagle deposit (viewed east).

¹ Minerals Division, Australian Geological Survey Organisation, GPO Box 378, Canberra, ACT 2601; tel. +61 2 6249 9713 (RB), +61 2 6249 9577 (DLH); fax +61 2 6249 9983; email Richard.Blewett@agso.gov.au, David.Huston@agso.gov.au.

Granitoid complexes and greenstone belts in the Pilbara Craton interpreted to extend down to the mid-crustal boundary at 14 km

Peter Wellman¹

The depth extent of outcropping major basement features, an important parameter for many geological applications (e.g., modelling mineral systems), is unknown for most areas in Australia. Whereas reflection seismic images show that granites and detachments have moderately shallow bases (5–10 km) in some

areas, geophysical evidence demonstrates that basement structures in the north Pilbara Craton extend to the base of the upper crust (14 km deep), and that the boundaries of the granitoid complexes are close to vertical.

The Pilbara Craton occupies an area (~650 × 500 km) of Archaean rocks in the

northern part of Western Australia. It is older (~3500–2800 Ma) than other areas of Australian crust, from which it differs structurally in consisting of mainly (60%) domal granitoid complexes 50–100 km diameter separated by synformal greenstone belts. The granitoid complexes have been formed by multiple intrusions

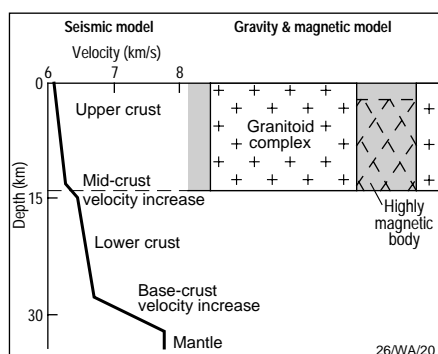


Fig. 14. Comparisons between the seismic refraction model and the gravity and magnetic model for the crust of the Pilbara Craton.

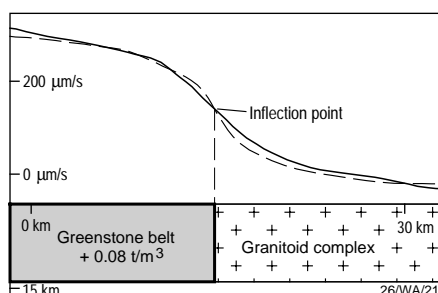


Fig. 15. An example of modelling the gravity gradient between a granitoid complex and greenstone belt (computed at lat. 21.4°S, long. 117.1°E). Observed profile, continuous line; modelled profile, dashed line.

over a long period, and parts are intensely deformed. The greenstone belts include a variety of sedimentary and intrusive rocks and felsic, mafic, and ultramafic lavas, and commonly reflect only greenschist metamorphic grade. This basement is in places overlain by Late Archaean and Permian–Tertiary cover rocks, but it forms extensive, largely unweathered outcrops in the north Pilbara Craton.

As a contribution to the joint AGSO–GSWA (Geological Survey of Western Australia) ‘North Pilbara’ project for the National Geoscience Mapping Accord, I have computed the depth extent of this basement from seismic refraction data, and gravity and magnetic anomalies (Wellman 1999: AGSO Record 1999/4).

Pilbara crustal modelling

According to Drummond (1983: BMR Journal of Australian Geology & Geophysics, 8, 35–51), seismic refraction data represent the Pilbara Craton as a two-layer crust in which the velocity increases gradually in the upper and lower parts and more sharply between them (Fig. 14). The crust thickens slightly to the south. The mid-crustal boundary averages ~14 km depth; and the base of the crust, ~30 km.

Granite–greenstone contacts have been geologically mapped in outcrop areas, and geophysically mapped (using short- and medium-wavelength magnetic anomalies) in subcrop areas. This contact is commonly irregular in plan at the outcrop/subcrop surface, and is likely to be equally irregular at deeper levels. The steepest gradient (inflection) of the gravity anomalies gives a smoothed estimate of the position of the granite margin about halfway down the side of the granite bodies (Fig. 15). This gra-

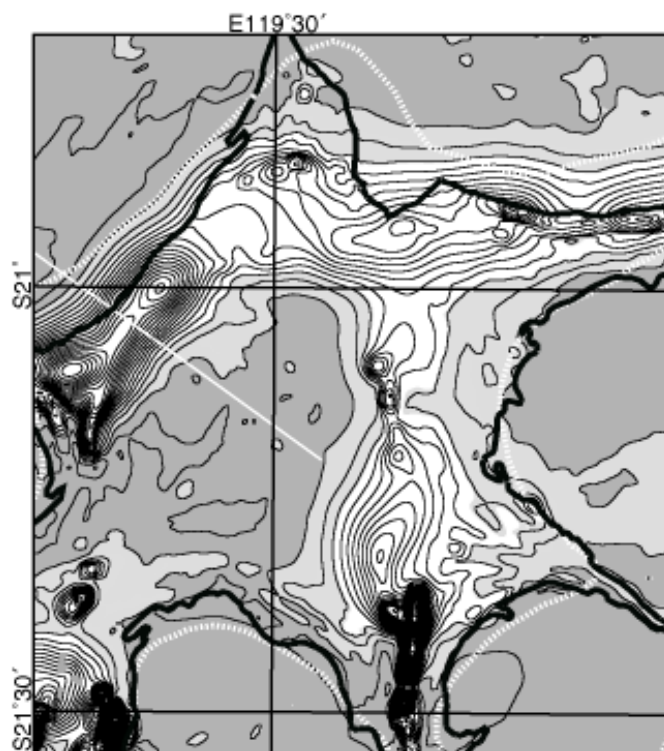


Fig. 16. Large magnetic anomalies expressed by greenstones in a 115 x 105-km area of the Pilbara Craton. Contours (at 250-nT intervals) show magnetic anomalies reduced to the pole on the assumption that the magnetic inclination is close to the near-vertical dip of the greenstones (i.e., 80°). Thick black lines trace the outcrop/subcrop contact between granitoid complexes and a greenstone belt. The white dotted line represents the steepest gravity gradient, showing the smoothed position of the margin of the granites at depth. The northwesterly oriented straight line in the west marks the position of the magnetic profile in Figure 17.

dient generally follows the average position of the mapped contact, so for most granites the margin slope averages near vertical.

The relative thicknesses of the granites can be determined from the residual gravity anomalies. The residual amplitudes of gravity lows over the granites are consistent for about two-thirds of the granites, which have a similar depth; the remainder are 80–50 per cent shallower.

The approximate thickness of the granitoid complexes and greenstone belts can be determined by 3D modelling the gravity gradient between them. A vertical boundary to 14 km depth between granitoid complex, represented by a prism, and greenstone belt produces a gravity anomaly consistent with the observed grid to within the accuracy of the 5-km-spaced observations. An example of this is shown in Figure 15.

In theory the depth to the base of the granite–greenstone layer can be calculated from the mean gravity difference and the mean density difference. However, both the mean density of the greenstone belts at the surface, and the change in the density difference with depth, are poorly known.

Very large, long-wavelength magnetic anomalies occur intermittently over the greenstones (Fig. 16). With an amplitude of 1000–3600 nT, width at half-amplitude of ~9 km, and strike length of 10–30 km, they are some of the largest in Australia. The mean depth to the top of these bodies is 1.5 km in the west and 2 km in the east. Modelling shows that the widths of causative bodies cannot be narrow, but must be similar to the anomaly

widths at one-half amplitude — generally about 9 km. The shapes of the tails of the anomalies are consistent with depths to the bases of bodies of 14 km (Fig. 17). The amplitudes of observed anomalies are consistent with an average apparent susceptibility that falls within the range of 0.05–0.2 SI units in the anomalous bodies. The only likely rock type fitting this profile in the Pilbara Craton is banded iron formation, whose bedding-parallel susceptibility is typically 0.5–2.0 (SI), ratio of remanent to induced magnetisation is typically 1–2, and susceptibility and remanence are both close to the plane of bedding owing to geometrical effects. Averaging the above susceptibility ranges (for the observed anomalies and bedding-parallel banded iron formation) implies that banded iron formation constitutes ~4 per cent of the volume of the greenstones.

Conclusion and implications of the Pilbara upper crustal model

Gravity and magnetic data for the Pilbara Craton are consistent with the structures of the Early Archaean basement extending down near-vertically, from the surface, to the base of the upper crust ~14 km deep.

This upper crustal model (Fig. 14) is an important constraint on models of geological evolution and mineral systems because it:

- defines the present shape of the geological elements (though it does not discriminate the mode of emplacement of the granitoid complexes);

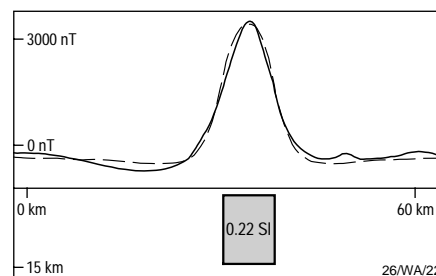


Fig. 17. An example of modelling the large magnetic anomaly over the greenstone belt in Figure 16 (q.v. for location of profile). Observed profile, continuous line; modelled profile, dashed line.

- shows that any low-angle detachment must be at the base of the upper crust or deeper (cf. Yilgarn Craton interpretations; Swager et al. 1997: Precambrian Research, 83, 43–56);
- shows that gravity and magnetic data can in certain circumstances reveal important information about the significance of the mid-crustal boundary;
- defines the depth extent of surface rocks, an important parameter for delimiting the volume of rock of various types that can be scavenged for metals by solution; and
- indicates that faulted margins between granites and greenstones extend to great depths, facilitating plumbing and fluid flow.

¹ Minerals Division, Australian Geological Survey Organisation, GPO Box 378, Canberra, ACT 2601; tel. +61 2 6249 9653; fax +61 2 6249 9983; email Peter.Wellman@agso.gov.au.

Stable isotopes — signposts for mineralisation

A new regional exploration tool

John F. Lindsay¹ & Martin D. Brasier²

Stable isotopes are a proven tool for assessing regional fluid-flow history in highly mineralised regions, such as the McArthur and Mount Isa Basins. Whereas past stable-isotope studies in such regions have focused on the orebodies or their surrounding geochemical halos, we have adopted a more holistic approach. In a recent study, we appraised the stable isotopes of carbon in carbonate rocks for discriminating primary isotopic signatures and correlating them in turn with basin-fill

architecture. By so doing, we have established a geochemical baseline against which the effects of mineralisation, especially fluid movement, can be compared. As a consequence of this work, we have accumulated an extensive database of carbon- ($\delta^{13}\text{C}_{\text{carb}}$) and oxygen- ($\delta^{18}\text{O}_{\text{carb}}$) isotope plus associated major- and trace-element analyses (Brasier & Lindsay 1998: *Geology*, 26, 555–558; Lindsay & Brasier in press: *Precambrian Research*).

Introduction

Since 1995, AGSO and Oxford University have been collaborating in an investigation of the use of stable-isotope chemostratigraphy for evaluating sediment-hosted metal deposits. This research is a contribution to the 'North Australian basins resource evaluation' project in the McArthur and Mount Isa Basins for the National Geoscience Mapping Accord (NGMA).

The stable isotopes, C^{13} and C^{14} , are fractionated during photosynthesis, and

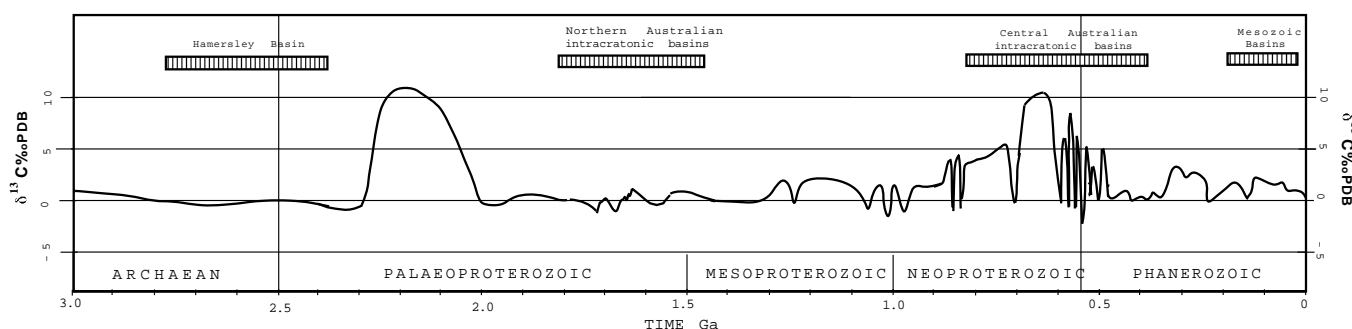


Fig. 18. Carbon-isotope ($\delta^{13}\text{C}_{\text{carb}}$) summary curve for the last 3 billion years of Earth history. Note the long period of low activity throughout the Palaeoproterozoic (adapted from Brasier & Lindsay 1998: op. cit.).

ultimately come into equilibrium with the global ocean. Their ratios, where preserved in carbonate rocks ($\delta^{13}\text{C}_{\text{carb}}$), provide an insight into biospheric activity, and record the rate at which organic carbon was being buried in sedimentary

basins (e.g., Des Marais et al. 1992: Nature 59, 605–609). The pattern of secular variation of $\delta^{13}\text{C}_{\text{carb}}$ for the last billion years of Earth history is now moderately well documented (Fig. 18). Major excursions of $>2\%$ have been documented glo-

bally. They represent significant events in the history of the Earth, particularly its biogeochemical evolution (for a summary, see Knoll & Canfield 1998: The Paleontological Society Papers, 4, 212–243). The Neoproterozoic–Phanerozoic

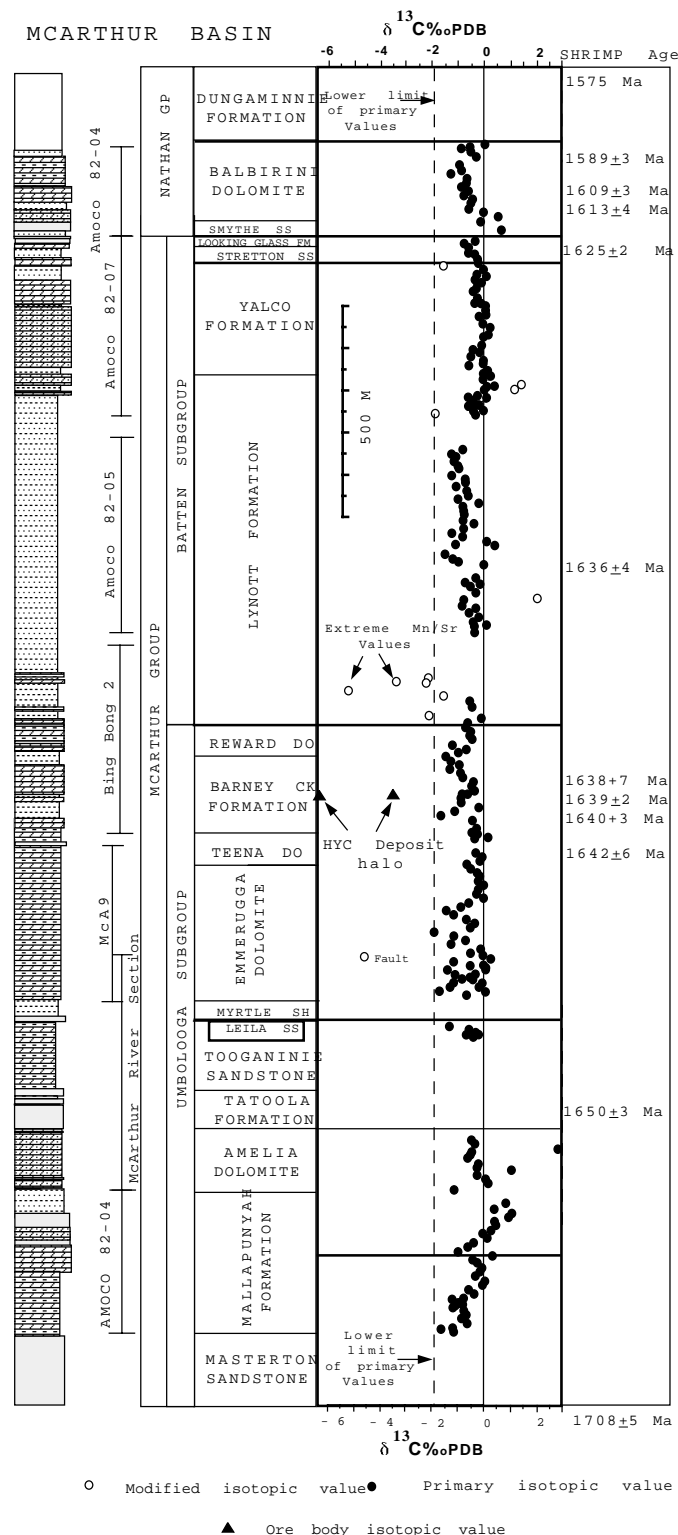


Fig. 19. Carbon-isotope ($\delta^{13}\text{C}_{\text{carb}}$) data from the main depocentre of the McArthur Basin (after Brasier & Lindsay 1998: op. cit.; Page 1997: AGSO Record 1997/12; Page & Sweet 1998: Australian Journal of Earth Sciences, 45, 219–232). Isotopic data for the HYC deposit from Rye & Williams (1981: op. cit.).

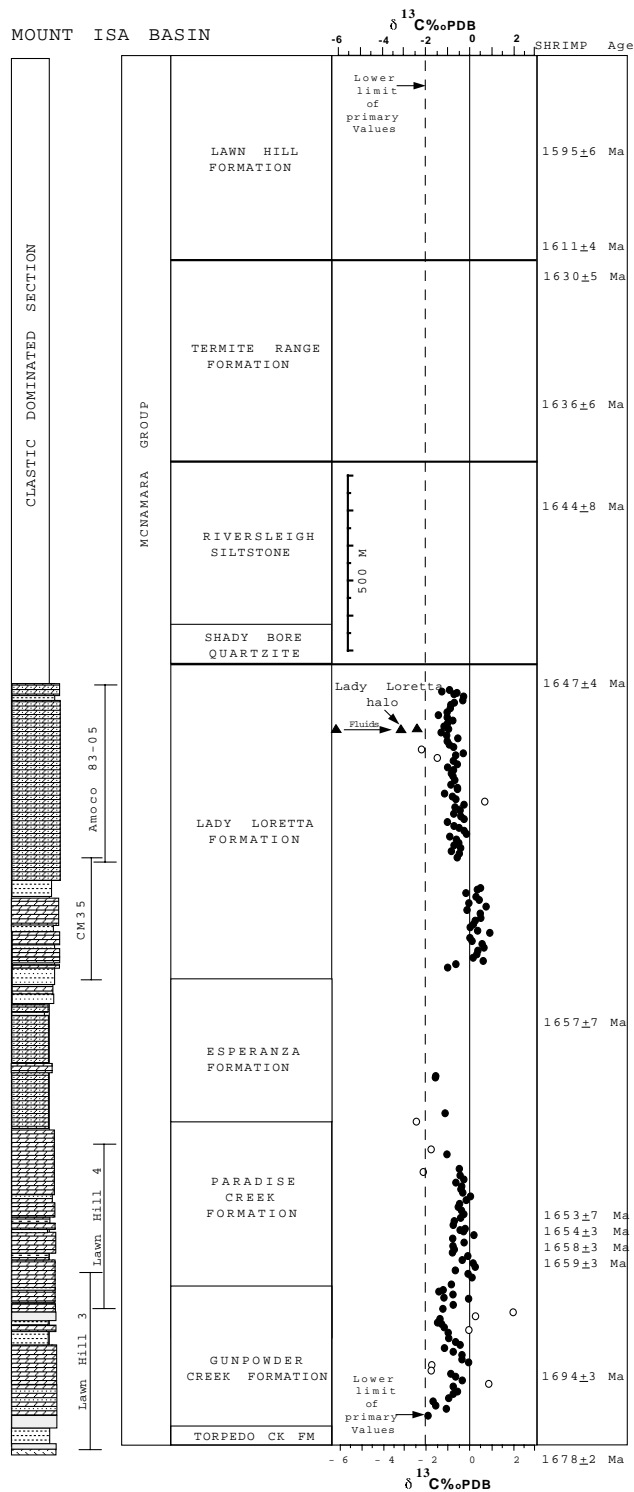


Fig. 20. Carbon-isotope ($\delta^{13}\text{C}_{\text{carb}}$) data from the main depocentre of the Mount Isa Basin (after Brasier & Lindsay 1998: op. cit.; Page 1997: op. cit.; Page & Sweet 1998: op. cit.). Isotopic data for the Lady Loretta deposit from McGoldrick et al. (1998: op. cit.).

transition, for example, was a time of major biological, geological, and environmental revolutions. These revolutions were accompanied by major changes in the carbon cycle that produced a distinctive secular carbon curve (Fig. 18), which has proved of value in regional correlation (e.g., Calver & Lindsay 1998: *Australian Journal of Earth Sciences*, 45, 513–532).

The rocks of the Palaeoproterozoic McArthur and Mount Isa Basins offered a major challenge — first, because so little was known about them; and, second, because of their antiquity. Initially, we were concerned that, since the rocks were so ancient, diagenesis may have altered the primary carbon-isotopic values and left little indication of oceanic history. However, after an extensive pilot study in 1995, during which 48 samples were analysed in great detail, we found that diagenesis had occurred early in the carbonate rocks; consequently, early fluid movements had been restricted, and primary carbon-isotopic signatures were preserved. Thereafter, we began a more extensive program of acquiring $\delta^{13}\text{C}_{\text{carb}}$ data for both the McArthur and Mount Isa Basins. We analysed the carbonate intervals in drillcore from the main depocentres and the margin or platform successions of both basins (Figs. 19 and 20), to evaluate the potential of the data for yielding pointers to mineralisation.

The dataset

To date we have analysed ~600 samples taken at 10-m intervals from more than 12 km of core from 15 major drillholes. The samples provide information for every carbonate interval in the McArthur and Mount Isa Basins' successions (Figs. 19 and 20). The data provide the most comprehensive and best dated $\delta^{13}\text{C}_{\text{carb}}$ stratigraphy yet obtained from such ancient rocks anywhere on Earth.

Analysis of the data produced some surprises, as the secular carbon curve ($\delta^{13}\text{C}_{\text{carb}}$) proved to be extremely flat (Figs. 19 and 20; Brasier & Lindsay 1998: *op. cit.*). The $\delta^{13}\text{C}_{\text{carb}}$ values from both basins vary within a narrow range — around a mean of -0.6‰ ; extreme values seldom lie farther than 1‰ from the mean. These results, combined with those from earlier studies on younger rocks (e.g., in the Bangemall Basin; Buick et al. 1995: *Chemical Geology*, 123, 153–171), imply that the global ocean reached a state of equilibrium in the mid-Palaeoproterozoic and remained stable for almost a billion years. Current models of the ocean suggest that

maintaining the carbon mass balance requires only minor tectonic activity. The implication that tectonic activity was moderate during this time is significant, as current plate-tectonic models suggest that it was a period of supercontinent assembly and dispersal (Hoffman 1989: *Geology*, 17, 135–138; Condie 1998: *Earth and Planetary Science Letters*, 163, 97–108). The results are, however, consistent with earlier AGSO work which supports a supercontinent model, but indicates that crustal evolution was anorogenic and plate motions slow (Wyborn 1988: *Precambrian Research*, 40/41, 37–60; Idnurm & Giddings 1988: *Precambrian Research*, 40/41, 61–88). Perhaps significantly, this period also coincides with the worldwide development of sediment-hosted Pb–Zn deposits.

Applications to exploration

Along with the more esoteric understanding of planetary history, there are clear pragmatic reasons for assembling a database of carbon and oxygen isotopes, for they can be used as vectors for mineralisation. Organic carbon is, of course, an important reductant in the deposition of some stratiform orebodies. During ore genesis, the isotopic ratios of both carbon and oxygen are altered, providing a useful indicator of the passage of mineralising fluids.

Williams (1978: *Economic Geology* 73, 1005–1035 and 1036–1056) first put forward the idea that the stratiform orebodies at McArthur River are not precisely syngenetic, but were deposited in response to early diagenesis in unconsolidated sediments. Detailed work on the highly mineralised zone associated with the Barney Creek Formation in the McArthur Basin (Rye & Williams 1981: *Economic Geology*, 76, 1–26; Hinman 1995: AGSO Record 1995/5; Lindsay & Brasier 1997: AGSO Record 1997/12) has shown that the passage of fluid can be detected as much as 40 km from the nearest known orebodies, and is directly controlled by the sequence stratigraphy. The passage of fluids depresses the $\delta^{13}\text{C}_{\text{carb}}$ curve by up to 10‰ (Fig. 19); the $\delta^{18}\text{O}_{\text{carb}}$ curve is similarly depressed. The data suggest that fluid movement was early, as Williams (1978: *op. cit.*) suggested, but did not occur until after the carbonates had been sealed diagenetically, such that they acted as aquicludes.

As a result of seismic interpretation bearing on the framework of the McArthur Basin, the stable-isotope data can place the movement of fluids in both spatial and

temporal contexts, and accordingly can be used as a predictive tool (Lindsay 1998: AGSO Record 1998/38).

In the Mount Isa Basin, McGoldrick et al. (1998: in Arehart & Hulston, Editors, 'Proceedings of the 9th International Symposium on Water–Rock Interaction', Balkema, Rotterdam, 561–564) have found distinctive isotopic signatures associated with the Lady Loretta deposit, including depressed carbon- and elevated oxygen-isotope values (Fig. 20). Farther afield, at Broken Hill, $\delta^{13}\text{C}_{\text{carb}}$ values in carbonates from the main lode are depressed dramatically to -22‰ (Yibao et al. 1987: *Transactions of the Institute of Mining and Metallurgy*, 96, B15–B30). The only other $\delta^{13}\text{C}_{\text{carb}}$ values that lie below -2.0‰ are from samples close to fault planes or major erosional surfaces that apparently have not been associated with mineralisation (Fig. 19).

Conclusions

The primary isotopic curves from Palaeoproterozoic successions are extremely flat. Consequently, an explorer in the McArthur and Mount Isa Basins can examine isotopic data from any carbonate interval without knowing its precise stratigraphic location, and quickly determine if mineralising fluids have passed it at some time in the past. As the primary carbon-isotope signature reflects the geochemistry of the ancient global ocean, it represents a tool that is not only of value to exploration in Australia but potentially has a global application.

Acknowledgments

We thank Aberfoyle Resources, Pasminco Exploration, and the geological surveys of Queensland and the Northern Territory for providing access to drillcore; Julie Cartlidge, John Pyke, and Owen Green for laboratory support; and Duncan Davidson and Kurt Barnett for assistance with gamma-ray logging of cores. John Lindsay thanks the former Australian Departments of Industry, Science & Tourism, and Primary Industries & Energy, for financial support while he was a visiting scholar at the Earth Sciences Department, Oxford University.

¹ Minerals Division, Australian Geological Survey Organisation, GPO Box 378, Canberra, ACT 2601; tel. +61 2 6249 9428; fax +61 2 6249 9956; email John.Lindsay@agso.gov.au.

² Earth Sciences Department, Oxford University, Parks Road, Oxford, OX1 3PR, UK; tel. +44 1865 27 2074; fax +44 1865 27 2072; email Martin.Brasier@earth.ox.ac.uk.

Some thermal consequences of high heat production in the Australian Proterozoic

Martin Hand¹, Mike Sandiford¹, & Lesley Wyborn²

The role of radiogenic decay in generating high-temperature thermal regimes in near-normal-thickness crust has been largely ignored. This oversight reflects a perception that radiogenic-heat-production concentrations are generally too low to generate significantly elevated conductive thermal regimes. However, in parts of the Australian Proterozoic, crustal (radiogenic) heat production that is largely concentrated in granites is roughly twice the world average for Proterozoic terranes. The existence of these anomalous heat-production concentrations in Australian Proterozoic rocks has important implications for generating high geothermal gradient regimes without appealing to external heat sources. The source region for most of these anomalously radiogenic granites was a lower crustal layer that was underplated from the mantle before 2000 Ma. Why this mantle event was so unusually enriched in K, Th, and U at this period of crustal evolution remains enigmatic.

Heat production in some Australian Proterozoic terrains

High-geothermal-gradient processes dominate the geological record in the Australian Proterozoic. These are principally expressed in the formation of regional high-temperature low-pressure metamorphic terrains (e.g., Mount Isa Inlier, northern Arunta Inlier, Broken Hill Block) and voluminous, crustally derived granitic magmatism. Considerable worldwide effort has been directed toward the study of high-geothermal-gradient regimes, principally because they are thought to represent significant departures from general notions of normal continental thermal conditions. For this reason, the advection of heat in the form of magmas is generally considered necessary to create a high-temperature regime in near-normal-thickness crust. While the advection of heat is likely to remain the governing paradigm for driving high-temperature low-pressure processes, the volume of synmetamorphic magmatism in some Australian high-temperature low-pressure metamorphic terrains (e.g., Broken Hill Block) appears too small to explain the observed metamorphism. Moreover, the application of the existing paradigm is challenged by sev-

eral important observations:

- regional high-temperature low-pressure metamorphism comprehensively postdates (>120 Ma) voluminous magmatism in the northern Arunta and western Mount Isa Inliers (Williams et al. 1996: *Journal of Metamorphic Geology*, 14, 29–47; Conners & Page 1995 *Precambrian Research*, 71, 131–153.);
- in the northern Arunta Inlier, high temperatures (>650°C) and low pressures (500 MPa) persisted for upwards of 25 Ma (Williams et al., 1996: op. cit.), far in excess of that expected for heating from a primary magmatic source, and imply that metamorphism occurred in quasicongruent equilibrium; and
- many of the voluminous Palaeo- and Mesoproterozoic granitic magmas derived from moderately shallow crustal sources do not appear to be associated with major mantle-derived magmatic events (Wyborn et al. 1998: in AGSO Record 1998/33, 47–59).

Despite the spatial association between granitic bodies and high-temperature low-pressure metamorphism in both the Mount Isa and northern Arunta Inliers, the interval between metamorphism and granite intrusion precludes advection as the primary heating mechanism. A notable feature of these terranes is that the heat-production capacity of premetamorphic granites is much higher (6–16 $\mu\text{W m}^{-3}$) than average for the crust. In the northern Arunta Inlier for example, granites with an average heat-production capacity of $\sim 7 \mu\text{W m}^{-3}$ crop out over at least 1200 km² (Fig. 21A) and form sill-like bodies up to 4 km thick, representing a depth-integrated heat flow of 20–25 mW m⁻². The generally high surface heat flows that characterise Australian Proterozoic terranes (average $\sim 80 \text{ mW m}^{-2}$; Cull 1982: *BMR Journal of Australian Geology & Geophysics*, 7, 11–21), coupled with the moderately thick mantle lithosphere (Zielhuis & van der Hilst 1996: *Geophysical Journal International*, 127, 1–16), suggest that the Australian Proterozoic crust generally contributes >50 mW m⁻² to the total surface heat flow (see also Taylor & McLennan 1985: table 5.5 in 'The continental crust: its composition and evolution', Blackwell Scientific

Publications, Melbourne), and up to 80 mW m⁻² in places such as the northern Flinders Ranges. These values are well in excess of the estimated normal crustal contribution to surface heat flow — <30 mW m⁻² (Taylor & McLennan 1985: op. cit.).

Heat-production concentrations of the magnitude of those in parts of the Australian Proterozoic have profound implications for mid-crustal thermal regimes. In a modelled steady-state thermal regime for a crustal section in the northern Arunta Inlier (Fig. 21B), an insulating sedimentary layer a few kilometres thick with a thermal conductivity of 2.25 W m⁻¹ K⁻¹ caps the bulk of the crust, which has an assumed thermal conductivity of 3 W m⁻¹ K⁻¹ and heat production linearly decreasing from a maximum of 3 $\mu\text{W m}^{-3}$ at the surface to 0.5 $\mu\text{W m}^{-3}$ at the Moho. Applying a basal heat flow of 20 mW m⁻² results in a maximum surface heat flow of around 110 mW m⁻², dropping to around 90 mW m⁻² in areas of lower heat production. Although these values are high, they are still within the present-day range observed in Proterozoic regions such as the Mount Painter and Tennant Creek Inliers (Cull 1982: op. cit.).

At a depth of 18 km, roughly coinciding with the level of denudation in the southeast Reynolds and Anmatjira Ranges, the maximum heat flow is around 65 mW m⁻². For the heat-production distribution shown in Figure 21A, steady-state temperatures are up to 720°C at 18 km depth. This compares with regional peak metamorphic temperatures at 1580 Ma in the order of 680–750°C at around 18 km depth in the southeastern Reynolds and Anmatjira Ranges and along the Yalarambi Range. These results suggest that the prolonged high geothermal gradient regime in the Reynolds Range (Williams et al. 1996: op. cit.) may have been largely generated by elevated levels of crustal heat production.

An important aspect of the thermal structure is the large vertical temperature gradients (up to 40°C km⁻¹) above the anomalous mid-crustal heat production. These large gradients reflect the extreme sensitivity of the thermal structure to the depth of burial of the heat-production layer. Additionally, they imply that moderately small differences in the depth of

denudation across a terrain will be reflected by large regional temperature gradients.

The magnitude of potential lower-crustal temperatures is strongly dependent on the thermal properties of the crust.

In particular, the thermal conductivity of a sedimentary layer blanketing the crust will have an important impact on lower-crustal temperatures. The average thermal conductivity estimate for sedimentary rocks in the Mount Isa region,

for example, weighted according to stratigraphic thickness of the component sequences is $\sim 2.6 \text{ W m}^{-1} \text{ K}^{-1}$ (MacLaren et al., submitted to *Geology*). The figure we chose ($2.25 \text{ W m}^{-1} \text{ K}^{-1}$; Fig. 21B) is based on the general results of conduc-

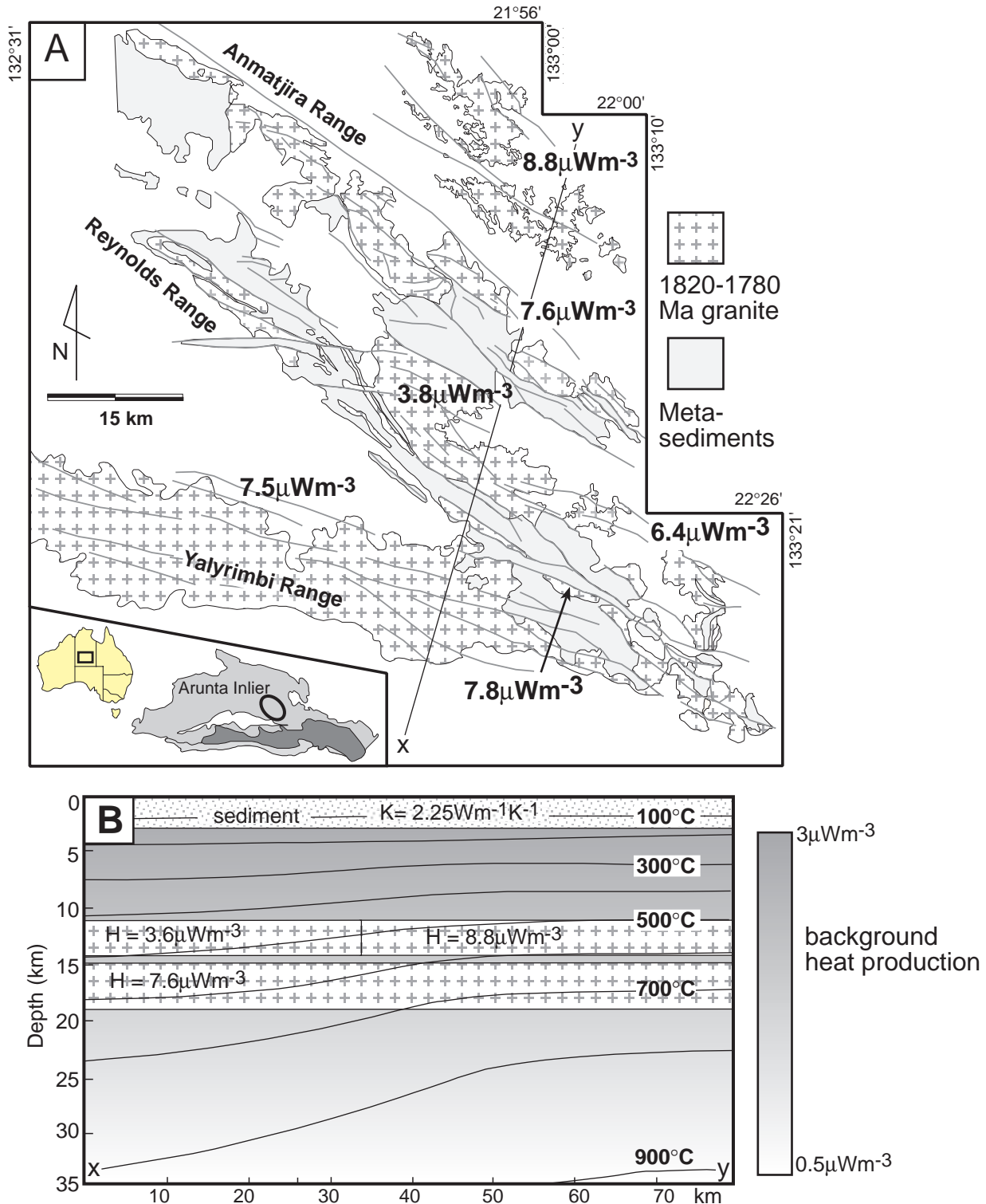


Fig. 21. (A) Distribution of high-heat-production granites in the Napperby region of the northern Arunta Inlier. (B) Steady-state thermal regime arising from burial of the anomalous heat production contained in the granites. This section approximates the pre-orogenic geometry based on field observations, including the movement of specific fault-blocks and the regional northward tilt. The heat production values are calculated for 1600 Ma, which roughly coincides with regional high-temperature low-pressure metamorphism.

tivity measurements. Increasing it by 25 per cent (to $2.8 \text{ W m}^{-1} \text{ K}^{-1}$) would result in a $\sim 40^\circ\text{C}$ decrease in calculated Moho temperature. Even so, the thermal conductivity of partly consolidated and diagenetic sediments may be 25–50 per cent less than their lithified equivalents (e.g., Griffiths et al. 1992: in 'Geological applications to wireline logs II', Geological Society, Special Publication 65, 299–315). Therefore, the average thermal conductivity of blanketing sedimentary layers may be much lower ($\leq 2.0 \text{ W m}^{-1} \text{ K}^{-1}$). This suggests that the presence of sedimentary basins in crust with anomalous heat production may exert an important control on the generation of high-geothermal-gradient regimes.

Implications for granite genesis

Since the thermal regime is sensitive to the depth of burial of anomalous heat production, restoring the heat-production content of the mid-crustal granites to likely pre-segregation depths should logically lead to lower-crustal temperatures exceeding the granitic solidus. This suggests that some granite formation may be largely the crustal response to conductive thermal regimes generated by deeply buried heat production. If heat-production concentrations of the order calculated for the northern Arunta Inlier were located near the base of crust greater than ~ 30 – 35 km thick, lower-crustal temperatures would exceed the bulk crustal liquidus. This would have profound mechanical consequences for Proterozoic tectonism (e.g., crustal convection). That these processes do not appear to have occurred to any great extent suggests that, in places such as the Arunta Inlier, the Proterozoic crust was moderately thin. This in turn implies that the voluminous granites that characterise many Australian Proterozoic regions were sourced from shallow depths ($\sim 35 \text{ km}$; Johannes & Holz 1996: 'Petrogenesis and experimental petrology of granitic rocks', Springer-Verlag, Berlin), an inference consistent with the Sr-depletion and Y-abundance of many of the Australian Proterozoic granites (Wyborn et al. 1998: op. cit.).

The removal of heat production from the lower crust during granite segregation has important long-term implications for the generation of further granite. The sensitivity of the thermal regime to the depth of burial of anomalous heat production means that segregation of U–Th–K-enriched granites from the lower crust leads to long-term lithospheric cooling. Thus the generation of additional granite

is inhibited by two factors: (1) cooler lower-crustal temperatures, and (2) the presence of a moderately anhydrous, refractory lower crust generated during earlier episodes of granite formation. This second point suggests that, unless fertile material can be added to the lower crust, successive generations of granite will require higher temperatures to form. Additionally, a consequence of the long-term cooling associated with the removal of lower-crustal heat production during granite segregation is that any additional melting events will increasingly require the input of external heat.

Wyborn et al. (1998: op. cit.) asserted that the temperatures of formation of Australian Proterozoic I-type granites continent-wide generally increased with time between 1880 and 1500 Ma. For the pre-1700-Ma granites, melting was dominated by minimum melt and biotite breakdown. Most granites formed after 1650 Ma are characterised by amphibole breakdown as the source temperatures reach $>1000^\circ\text{C}$. These higher-temperature granites are represented in the Cu–Au-associated Williams Batholith (Cloncurry area, Qld) and the Hiltaba Suite (Gawler Craton, SA). Further, a plot of Sm–Nd model ages (Fig. 22) shows that granites emplaced between 1500 Ma and 1900 Ma have Model T_{DM} ages $>2000 \text{ Ma}$, suggesting that very little material was added to the base of the crust after about 2000 Ma.

Therefore, granite production ceased in most of the Palaeoproterozoic provinces by about 1500 Ma, when either fertile source material was completely depleted and/or the higher temperatures required to generate the granites could not be reached.

While the anomalously high-heat-production concentrations are likely to have played a central role in the evolution of the Australian Proterozoic, a fundamental question that is yet to be fully resolved is the reason for the primary enrichment of heat-producing elements to levels up to three times that of normal crust. The Sm–Nd data (Fig. 22), combined with seismic refraction evidence (Goncharov et al. 1997: AGSO Research Newsletter 26, 13–16), suggest that these high values come from mantle-derived material that underplated the lower crust before 2000 Ma. Why this underplate was so enriched at this period of Earth evolution is yet another question awaiting a satisfactory answer.

Acknowledgments

Discussions with Sandra McLaren and Narelle Neumann are gratefully acknowledged as are reviews by Dave Champion and Alan Whitaker. Sue Edgecombe and Shen-Su Sun kindly provided Figure 22. Further information on this, and related topics can be found on the Internet at <http://jaeger.geology.adelaide.edu.au/research.html>.

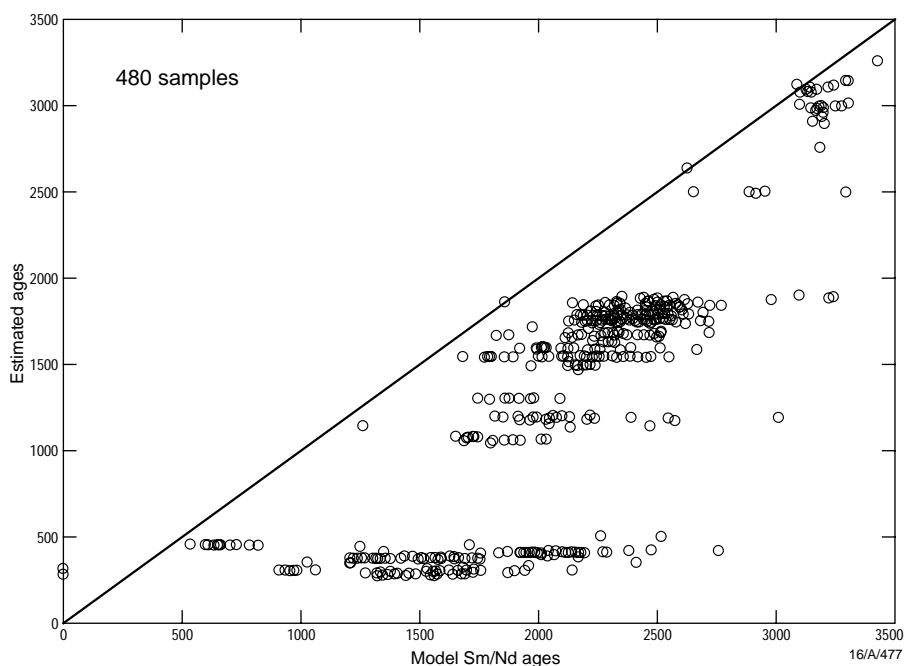


Fig. 22. Model Sm–Nd ages for Australian felsic igneous rocks vs estimated ages (mostly based on zircon ages). Note most samples indicate a pre-existing crustal history and that the bulk of felsic igneous rocks aged between 1900 Ma and 1500 Ma come from source material that is $>2000 \text{ Ma}$. All data are from OZCHRON, AGSO's geochronology database.

¹ Department of Geology and Geophysics, Adelaide University, Adelaide, SA 5005; tel. +61 8 8303 5841 (MH), +61 8 8303 5326 (MS); fax +61 8303 4346; email mhand

@geology.adelaide.edu.au, msandifo@geology.adelaide.edu.au.

² Minerals Division, Australian Geological Survey Organisation, GPO Box 378, Canberra,

ACT 2601; tel. +61 2 6249 9489; fax +61 2 6249 9983; email Lesley.Wyborn@agso.gov.au.

Interactive processing of mineral resource and occurrence data by Web users

Brian G. Elliott¹

Scientists in AGSO's Mineral Resources & Energy Program (formerly part of the Bureau of Resource Sciences) have developed a minerals and energy resources and locations information system — MINERALIS — which provides interactive facilities via the intranet for AGSO's resource geologists. A proposal to make it accessible to other users via the Internet is currently being developed.

MINERALIS is a second-generation database developed from two databases that AGSO initiated a decade ago: MINLOC (mineral occurrence locations) and MINRES (mineral resources), which were publicly released in October 1990 and February 1996 respectively. Integrating them in 1997–98 has facilitated streamlined data entry, processing, and reporting.

Development of MINERALIS with new Internet technologies and Oracle version 8 began in late 1997. Database specialists and users reviewed MINRES and MINLOC, and eliminated non-core attributes before they designed and coded the system. MINLOC and some MINRES data were then transferred to MINERALIS for user acceptance testing before the system was released for internal use in November 1998. Mineral occurrence and

resource data for the current year are now being entered.

As well as facilitating the entry, maintenance, and reporting of mineral occurrence and resource data, MINERALIS can also do complex calculations to meet AGSO's particular requirements, and tasks that were too difficult and/or too time-consuming for its parent databases. Now, using MINERALIS, resource geologists can routinely process industry data, so as to separate contained reserves from resources and allocate national resources according to AGSO classification criteria at levels of accuracy and consistency not always achievable before. MINERALIS also introduces an advanced reporting capability that tracks reasons for change in national resource inventories. This facility allows experienced users to make the incisive analyses needed — for example — for AGSO's input to national resource accounting carried out by the Australian Bureau of Statistics.

AGSO plans to use Web-based GIS and forms-technologies for making mineral occurrence and resource data publicly accessible via the Internet. A start has already been made. Maps showing mineral occurrences and resources are available on the AGSO website at <http://www.agso.gov.au/map/TOC.html> and

<http://www.agso.gov.au/ngis/locator.html>. Clients will be able to download the latest MINLOC and MINRES product releases from the MINERALIS home page later this year. The system will give clients online access to the most up-to-date information. These clients in turn could help improve the size and quality of data holdings through interactive data entry facilities via the Internet.

MINERALIS will also be able to link all State departments of mines and AGSO via the Internet. AGSO has discussed with State government colleagues the concept of using MINERALIS to jointly capture and share mineral deposit and occurrence data. The link would offer opportunities to collaborate more closely, develop better data standards, and share data-entry and data-maintenance workloads in these times of downsizing and fast depleting staff resources. Queensland's Department of Minerals & Energy and AGSO are exploring the possibility of connecting a workstation located in the Department to MINERALIS via the Internet.

¹ Mineral Resources & Energy Program, Australian Geological Survey Organisation, GPO Box 378, Canberra, ACT 2601; tel. +61 2 6272 4433, fax +61 2 6272 4161, email Brian.Elliott@agso.gov.au.

Post-intrusion heating associated with high-heat-producing Proterozoic granites — implications for mineralisation?

Sandra McLaren¹, Narelle Neumann¹, Mike Sandiford¹, & Lesley Wyborn²

Mineral deposits in Australian Proterozoic terrains are commonly associated spatially and temporally with granitic intrusives. Accordingly, the granites are perceived as the sources of advective heat and metal-bearing fluids in the mineralisation process. In places, however, mineral deposits are as much as 40 m.y. younger than a spatially associated intrusive, and the origin of their mobilising and transporting fluid(s) remains enigmatic. We propose a model in which radiogenic decay may initiate a second stage of hydrothermal circulation, and thus create an alternative mechanism for mineralisation that is spatially asso-

ciated with Proterozoic granites. This model also contributes to the debate about why certain fluids spatially associated with granite intrusives have a mainly 'magmatic' character, while others in the same area have properties that are better classified as 'meteoric', 'metamorphic', or 'basinal'.

Fundamentals of a prolonged-heating model

Australian Proterozoic granites are characterised by elevated to extreme enrichments of the heat-producing elements — U, Th, and K. Although this phenomenon is not confined to Austral-

ian examples, the level of enrichment in terrains such as the Mount Isa, Pine Creek, and Mount Painter Inliers is anomalous on a global scale (Table 2). As granites within these terrains retain a primary igneous Th:U ratio of ~3.5–4.5 (Durrance 1986: 'Radioactivity in geology: principles and applications', Halstead Press, New York), their high heat production is not simply a result of post-crystallisation alteration. Accordingly, we suggest that the intrusion of such enriched granites results in two hydrothermal circulation mechanisms due to:

- advective heat during intrusion; and
- prolonged radiogenic decay of heat-

producing elements in the granite.

Regardless of the source area, the intrusion of an anomalously radiogenic granitic magma results in fundamental changes to the crustal thermal structure, both above and below the intrusive level. The specific thermal effects will depend primarily on the total radiogenic heat production of the granite, but also on the depths of the magma source and intrusion and their relative length scale (i.e., the ratio of the width of the intrusion to the width of the source). The additional heat flowing from the mantle will also contribute to the thermal effects. Our qualitative modelling relates to the instantaneous emplacement of a magma (a reasonable approximation, as magmas must ascend fast enough to prevent conductive heat loss) in the upper crust at a depth of ~12 km (Fig. 23).

As a consequence of an intruding magma, advection causes a local transient thermal perturbation immediately around it. This is the mechanism by which classic metamorphic aureoles are formed, and may also give rise to what are loosely termed 'thermal-aureole Au deposits' (Wall & Taylor 1990: Geological Society of Australia, Abstracts, 25, 264–265). The intrusion of a granite of 'Williams Batholith-like' characteristics from a lower-crustal source causes an advective thermal anomaly (T_a , Fig. 24A) that extends only ~5 km from the granite margin and lasts for only ~2–4 m.y. After this time, in the absence of other heat sources, the system will rapidly return to steady-state background temperatures.

However, for granites with high concentrations of U, Th, and K, the decay of these radiogenic elements causes a second stage of heating (T_R , Fig. 24B; Fig. 25). This produces a prolonged broad thermal perturbation which is recorded up to 10 km from the granite margin. This heating has a low intensity (an additional ~40°C above background immediately surrounding the granite, and up to an extra 15°C ~10 km from the margin), but may be sustained for up to 300 m.y.

Hydrothermal fluids may circulate in response to thermal gradients within porous media. The long-term upper-crustal heating induced by radiogenic decay sustains locally elevated geothermal gradients, promoting circulation of hydrothermal fluids long after the intrusion of the magma. The potential to establish such enduring and extensive fluid-circulation systems at elevated temperatures has important implications for the leaching and deposition of metals.

Table 2. Geochemistry and present-day heat production

Granite unit	U (ppm)	Th (ppm)	K ₂ O (wt%)	Th:U	Q ($\mu\text{W m}^{-3}$)*
Average granite	4	15	3.5	3.8	2.5
MII — Williams Batholith	13	55	3.9	4.3	7.8
MII — Naraku Batholith	10	57	3.5	5.7	7.1
MII — Sybella Batholith	8	35	5.1	4.3	5.1
PCI — Cullen Batholith	9	39	5.0	4.1	5.8
PCI — Burnside Granite	17	48	5.5	2.8	8.4
MPI — Terrapinna Granite	9	55	5.6	5.9	7.0
MPI — Mount Neill Granite	19	67	3.5	3.5	10.2

Q = present heat production, calculated from present concentrations of U, Th, and K.

MII = Mount Isa Inlier, PCI = Pine Creek Inlier, MPI = Mount Painter Inlier. Average granite values are from Fowler 1990 ('The solid Earth', Cambridge University Press, New York). MII data from Wyborn et al. 1988 (Precambrian Research, 40/41, 509–541). PCI data from AGSO's ROCKCHEM database.

* As radioactive decay causes a reduction in the concentration of heat-producing elements through time, the value of the calculated heat production at the time of intrusion of each batholith would have been on average ~25–30% higher than the present day value quoted above; thus, when it intruded at 1670 Ma, the Sybella Batholith's heat production would have been 6.8 (compared with its current 5.1) $\mu\text{W m}^{-3}$.

Application of the prolonged-heating model to thermal-aureole gold deposits

In the eastern Mount Isa Inlier, the Ernest Henry, Starra, and Mount Elliott Cu–Au deposits are adjacent to the high-heat-producing Williams and Naraku Batholiths (Table 2). Within analytical error, the mineralisation at both Mount Elliott and Starra was essentially coeval with batholith emplacement (ca 1510–1485 Ma; Perkins & Wyborn 1998: Australian Journal of Earth Sciences, 45, 233–246). However, mineralisation at Ernest Henry, and some of the regional alteration within the Williams and Naraku Batholiths, followed granite intrusion by as much as 20 m.y. (Perkins & Wyborn 1998: op. cit.).

Similarly in the Pine Creek Inlier, the emplacement of the Cullen Batholith ($H = 5.8 \mu\text{W m}^{-3}$) preceded spatially related tin deposition by ~20 m.y., and gold mineralisation by ~40 m.y. (Klominsky et al. 1994: 'Radiothermal granites of the Cullen Batholith and associated mineralization', Czech Geological Survey, Special Papers, 5). According to Klominsky et al. (1994: op. cit.) and Partington & McNaughton (1997: Chronique de la Recherche Minière, 529, 25–44), mineralisation in this terrain was a multistage process, principally involving hydrothermal mobilisation related to the internal heat of the batholith, rather than its advective heat.

In addition to accounting for the time delay between intrusion and mineralisation in these examples, the results of 2D finite-element modelling presented here also explain the close spatial relationship between mineral deposits and these high-heat-producing granites. For

example, in the Pine Creek Inlier, gold has been deposited as a halo about 5 km from the margin of the Burnside Granite (Stuart-Smith et al. 1993: 'Geology and mineral deposits of the Cullen Mineral Field, Northern Territory', AGSO Bulletin 229). Thermal effects due to magmatic heating are minimal at these distances (Fig. 24A), but prolonged heating due to radiogenic decay may be significant.

Application of the prolonged-heating model to other deposit styles

High-heat-producing granites may also contribute to the formation of other styles of mineral deposit that are commonly related to basinal or low-temperature metamorphic processes. The Mount Isa Cu deposit, for example, occupying a greenschist-facies terrane, and the high-heat-producing Sybella Batholith, in an amphibolite-facies terrane, are juxtaposed either side of the Mount Isa Fault. This Cu deposit formed at ~1523 Ma, which is essentially coeval with the Isan Orogeny (Perkins et al. in press: Economic Geology) but much younger than the emplacement of the Sybella Batholith (~1670 Ma; Page & Bell 1986: Journal of Geology, 94, 365–379). Hydrothermal fluids deposited the Mount Isa copper at ~300°C (Heinrich et al. 1995: Economic Geology, 90, 705–730), but their circulation must have been activated by a mechanism other than the high-grade metamorphism in the adjacent terrain, which was uplifted to its present position no earlier than 1460 Ma (Perkins et al. in press: Economic Geology). Instead, regional-scale convection cells due to low-amplitude radiogenic heating in the Sybella Batholith may have provided the driving force for the mineralisation.

McLaren et al. 1998 (Geological Society of Australia, Abstracts, 49, 305) assert that the high geothermal gradients associated with the Isan Orogeny in the area adjacent to the Mount Isa Cu deposit were simply due to the known radiogenic-heat capacity buried in the crust without any additional advective component.

Solomon & Heinrich (1992: *Exploration Mining Geology*, 1, 85–91) have also suggested that radiogenic heat played a role in the generation of the associated Mount Isa Pb–Zn deposits.

Discussion

These examples provide an insight that may help to explain both the close spa-

tial and temporal relationships between Proterozoic mineralisation and radiogenic granitic intrusion. Importantly, this need not necessarily be a strictly temporal association. Secondary or later hydrothermal circulation cells developed above and adjacent to granite are simply responding to long-term crustal heating due to radiogenic decay within the granite. Fluids associated with these later hydrothermal circulation cells will have an increasingly meteoric or metamorphic character and may overprint earlier fluid events that are more magmatic in character. This explanation contributes to the current debate as to whether fluids associated with mineral districts that spatially

Fig. 23 (top left). Schematic-model x–y section showing the parameters and geometry used for the finite-element model discussed in the text. The crustal section, in the semi-infinite half-space as shown, is 40 km thick and 120 km wide. After the melting of a lower crustal source, a magma 4 km thick and 20 km wide intrudes the upper crust at a depth of 12 km. We then follow the thermal evolution of this magma during and after crystallisation for a period of 300 m.y. Owing to its greater volume (40×10 km), the source is characterised by a lower volumetric heat production than the product melt. The background, on which the source and intrusion are superposed, is characterised by an exponentially decaying (Lachenbruch-like) heat-production distribution with a characteristic length scale of decay of 22.5 km and an integrated contribution to the surface heat flow (q_c) of 45 mW m^{-2} . The mantle contribution to surface heat flow (q_m) is constant at 20 mW m^{-2} , and the thermal conductivity, considered to be depth-independent, is taken to be $2.5 \text{ W m}^{-1} \text{ K}^{-1}$. All temperature–time–path sites are at a depth of 12 km (corresponding to the depth centre of the pluton) and at varying distances from the pluton centre (10, 20, 25, 30, and 40 km); the individual temperature–time paths for these points are shown in Figure 24.

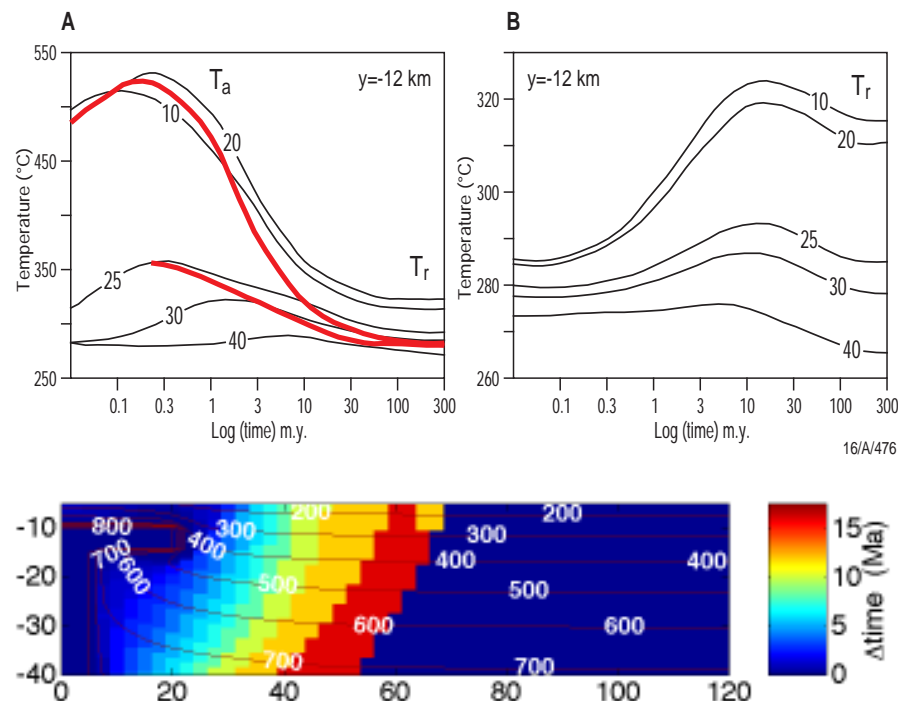
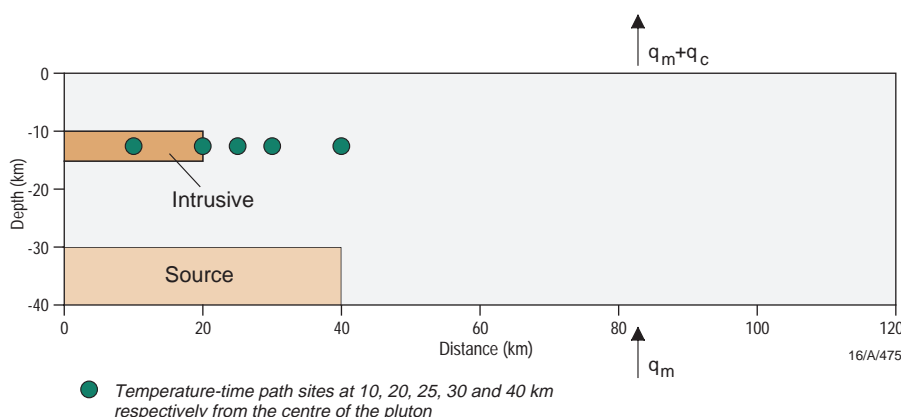


Fig. 25. Model x–y section contoured for temperature and also for the time (in m.y.) post-intrusion that various sections of the crustal column attain their maximum temperature. For example, the granitic body itself attains maximum temperature at the time of intrusion ($\Delta\text{time} = 0$ m.y.). At a distance of 10–20 km from the pluton margin, however, maximum temperatures are not attained until 5–10 m.y. after intrusion; this is the result of the additional phase of heating caused by radiogenic decay (Tr).

Fig. 24 (centre left). Temperature–time paths for the thermal model. Each path corresponds to a depth (y) of 12 km (adjacent to the heat-production maximum) and to points at lateral distances of 10, 20, 25, 30 and 40 km, as labelled, from the centre of the granite. Parameters are shown in Figure 23. (A) Both the thermal anomaly due to advective heat associated with intrusion (T_a) and subsequent radiogenic heating (Tr) associated with 'typical' Mesoproterozoic granite. The advective thermal anomaly (in the absence of any additional radiogenic heating component) is also shown (in red) for the 20- and 25-km temperature–time–path sites. This advective thermal anomaly is sustained for only ~3 m.y. after intrusion, and is not recorded in rocks more than ~5 km from the pluton margin (as indicated by the difference between the 25- and 30-km paths). (B) The radiogenic thermal anomaly (ignoring the initial advective response) shows a 30–40°C increase in temperature from that which would result from advective heat alone. Heating due to radiogenic decay reaches a maximum ~10 m.y. after intrusion, but is sustained well above the background temperatures for up to 300 m.y. (note logarithmic scale). The long-term cooling apparent some distance away from the intrusion (i.e., 40-km path) is a result of the upward movement of heat-producing elements from the source into the intrusion. This effect contributes to elevated lateral thermal gradients which may promote fluid circulation.

are related to granites will exhibit a magmatic or meteoric/basinal/metamorphic signature (e.g., Tennant Creek, Telfer, Tanami).

Hence, as a result of a single intrusive event there are two possible mechanisms for generating fluid circulation and thus facilitating ore precipitation. The first occurs almost instantaneously after intrusion, and is driven by advective heat. The second is driven by subsequent radiogenic decay in the granite, and has

the potential to be maintained for up to 300 m.y. Once radiogenic hydrothermal activity has been initiated, the potential for mineralisation then depends on other factors — including the presence of a source of metals, and specific fluid pathways and depositional conditions.

The modelling presented above demonstrates that a radiogenic heat source in the local environment cannot be underestimated.

¹ Department of Geology and Geophysics, University of Adelaide, SA 5005; tel. +61 8 8303 5376; fax +61 8 8303 4347; email msandifo@geology.adelaide.edu.au, smclaren@geology.adelaide.edu.au, nneumann@geology.adelaide.edu.au

² Minerals Division, Australian Geological Survey Organisation, GPO Box 378, Canberra, ACT 2601; tel. +61 2 6249 9489; fax +61 2 6249 9983; email Lesley.Wyborn@agso.gov.au.

The Kombolgie Subgroup — a new look at an old ‘formation’

I.P. Sweet¹, A.T. Brakel¹, & L. Carson²

Rocks that we assign to the Kombolgie Subgroup (Fig. 26) underlie the Arnhem Land Plateau, and form the Arnhem Land escarpment in Kakadu National Park. Named the Kombolgie Formation during the first systematic regional geological mapping of the Pine Creek region in the 1950s (synthesised by Walpole et al. 1968: BMR [AGSO] Bulletin 82), these rocks were mapped in greater detail during the reappraisal of the Katherine–Darwin region in the 1970s to 1980s by BMR (AGSO’s predecessor; e.g., Needham 1988: BMR [AGSO] Bulletin 224). More recently, the unit has been re-examined during joint NTGS (Northern Territory Geological Survey)–AGSO remapping of Arnhem Land and adjacent areas under the auspices of the National Geoscience Mapping Accord (NGMA). Stratigraphic, sedimentological, and geochronological studies have shed new light on these rocks. The unit now has better defined age constraints, and its nomenclature has been revised to reflect some of the complexities of its stratigraphic evolution. As a result, the former *Kombolgie Formation* has been elevated in rank to the *Kombolgie Subgroup*.

Stratigraphy and nomenclature — new results

The Kombolgie Subgroup, a quartz sandstone–conglomerate–basalt unit forming the basal part of the Palaeoproterozoic Katherine River Group, is the oldest component of the northwest McArthur Basin. This unit has been progressively more rigorously defined as new information on lithologies and relationships be-

came clear (Fig. 27).

The initial systematic work of Walpole (1962: ‘Mount Evelyn, NT — 1:250 000 Geological Series, SD/53–5’, BMR [AGSO], Canberra) and Randal (1963: ‘Katherine, NT — 1:250 000 Geological Series, SD/53–9’, BMR [AGSO], Canberra) was varied in only a minor way by Roberts & Plumb (1965: ‘Mount Marumba, NT — 1:250 000 Geological Series, SD/53–6’, BMR [AGSO], Canberra), who assigned glauconitic sandstones at the top of the ‘Kombolgie Formation’ to a separate formation — the McKay Sandstone.

Major advances in understanding the stratigraphy of this northern marginal part of the McArthur Basin were made by Needham & Stuart-Smith (1985: Australian Journal of Earth Sciences, 32, 219–230), particularly with regard to the relationships within a complex of coarse clastics and volcanics underlying the Kombolgie unit; Walpole et al. (1968: op. cit.) had included some components of these in the ‘Kombolgie Formation’. Recognising an unconformable relationship, Needham & Stuart-Smith (1985) assigned the older rocks to two newly defined groups — the Edith River and El Sherana Groups. They also introduced the widely used informal labels, Phk₁ and Phk₂, for the lower and upper Kombolgie sandstones, respectively; identified a local unconformity between the Nungbalgarri Volcanic Member and Phk₂; and mapped Phk₂ overlapping Phk₁ onto rocks of the Pine Creek Inlier.

In remapping the Milingimbi Sheet area (SD53–2), Carson et al. (in prep.: 1:250 000 Geological Map Series explana-

tory notes, NTGS–AGSO) have formalised a new nomenclature. They have raised the ‘Kombolgie Formation’ to Subgroup status; formally named and redesignated as formations the informal members, Phk₁ and Phk₂; redesignated the Nungbalgarri member as a formation; and incorporated the McKay Sandstone into the Kombolgie Subgroup (Fig. 27). Regional unconformities apparently truncate both the Nungbalgarri Volcanics and Gilruth Volcanic Member.

This nomenclature has been extended southwards (e.g., Sweet et al. 1999: ‘Mount Marumba SD53–6 — 1:250 000 Geological Map Series explanatory notes’, NTGS–AGSO), and is applicable throughout the whole outcrop belt of the Kombolgie Subgroup.

Age

In the first systematic isotopic geochronology in the McArthur Basin, the Katherine River Group (KRG), of which the Kombolgie Subgroup is a part, was bracketed between 1790 and 1520 Ma on the basis of K–Ar dating by McDougall et al. (1965: Journal of the Geological Society of Australia, 12, 67–90). The first dating to focus on the Kombolgie unit (Page et al. 1980: in ‘Uranium in the Pine Creek Geosyncline’, International Atomic Energy Agency, Vienna, 39–68) defined a lower age limit of 1688 Ma (Rb–Sr age of the Oenpelli Dolerite, which was interpreted as being overlain unconformably by the Kombolgie unit) and an upper limit of 1648 Ma (the minimum age for the then ‘Nungbalgarri Volcanic Member’ of the ‘Kombolgie Formation’).

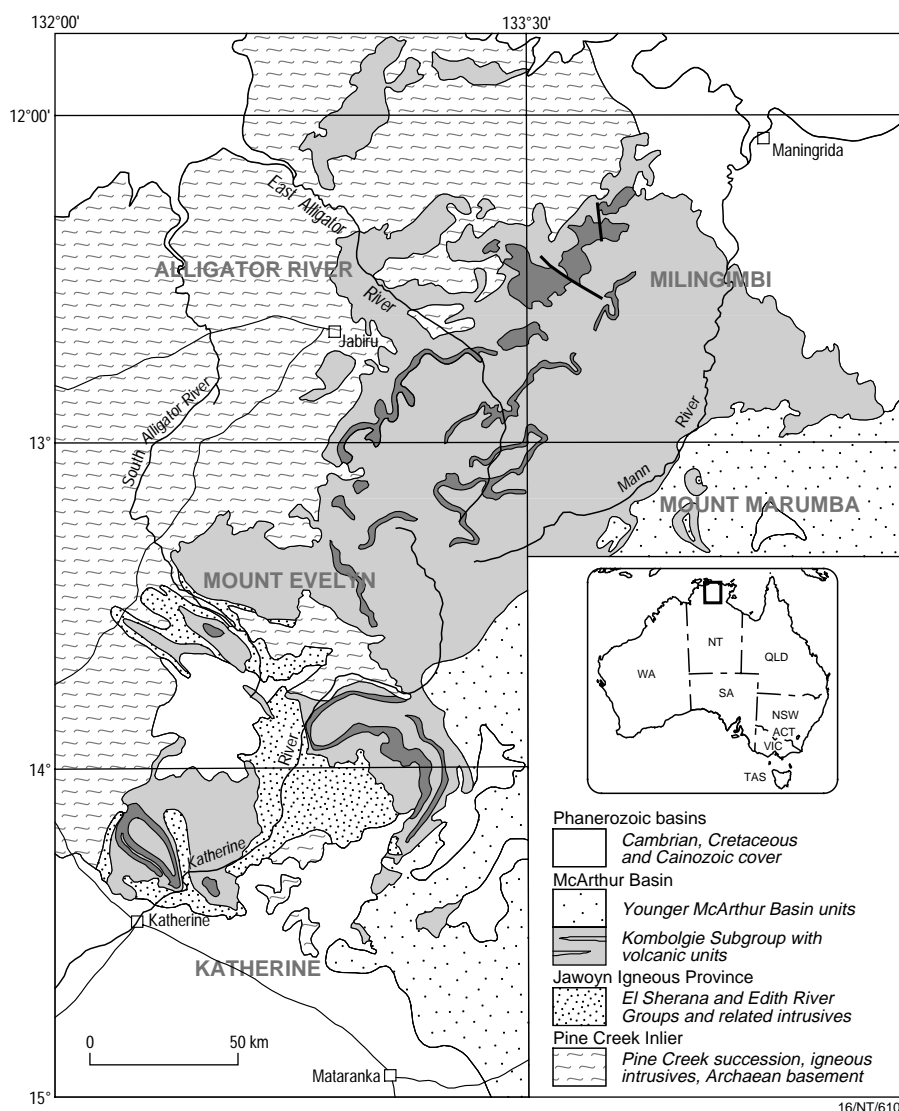


Fig. 26. Location map for outcrops of the Kombolgie Subgroup.

Since then, single-crystal U–Pb SHRIMP dating of zircons from the Plum Tree Creek Volcanics, which are clearly overlain unconformably by the Kombolgie Subgroup, has yielded an age of 1822 Ma (R.W. Page, quoted in Kruse et al. 1994: ‘Katherine SD53–9 — 1:250 000 Geological Map Series explanatory notes’, NTGS–AGSO). Three separate SHRIMP zircon ages provide a minimum age for the Kombolgie Subgroup:

- the West Branch Volcanics, at the top of the KRG and some 1000 m stratigraphically above the Kombolgie Subgroup in the Katherine area, are 1705–1712 Ma old (Page, in Kruse et al. 1994: op. cit.);
- the Jimbu Microgranite (Rawlings & Page 1999: Precambrian Research, 94(3–4), 225–250), which intrudes the upper KRG, has been dated at 1720 Ma, thus providing a reliable minimum age

- for the Kombolgie Subgroup; and a slightly tighter constraint on the minimum age is based on the correlation of the McCaw Formation, some 500 m stratigraphically higher in the upper KRG, with the Wollgorang Formation in the Tawallah Group (southern McArthur Basin); felsic volcanics in the lower Wollgorang Formation have been reliably dated at 1729 ± 4 and 1730 ± 3 Ma by Jackson et al. (1997: AGSO Research Newsletter 26, 20–22).

The age of the Kombolgie Subgroup is thus firmly constrained between 1822 and 1720 Ma — ~100 Ma (and more) older than previously believed — and cannot be an equivalent of the McArthur Group (as asserted by Plumb 1985: Precambrian Research, 29, 303–329), which is firmly established as being younger than about 1700 Ma (Page & Sweet 1998: Australian

Journal of Earth Sciences, 45, 219–232). Since the Subgroup forms the basal part of the KRG, its age is probably closer to 1800 Ma than to the upper limit of ~1720 Ma.

Sedimentology and environmental studies

Walpole et al. (1968: op. cit.) regarded the Kombolgie unit as being deposited under ‘shelf conditions’ (i.e., in a marine environment), but subsequent workers generally interpreted the depositional environment as fluvial (e.g., Needham 1984: ‘Alligator River, SD/53–1 — 1:250 000 Geological Series explanatory notes’, BMR [AGSO], Canberra). This interpretation is largely based on the general aspect of the sediments — strongly cross-bedded pebbly sandstone — and on a sedimentological study of the (now) Mamadawerre Sandstone by Ojakangas (1979: US Department of Energy report GJBX–173(79), 1–37), who concluded that the rocks were the product of a braided fluvial system with mainly east to south-east sediment transport across a broad braid plain sourced from the west to north-west.

Our work has shown significant departures from this model. For example, in the Katherine 1:250 000 Sheet area, Kruse et al. (1994: op. cit.) noted a strong south to southwest component in the upper part of the Subgroup, indicating transport from the northeast, and a similar pattern is evident in Mount Marumba (Sweet et al. 1999: op. cit.). In Milingimbi, Carson et al. (in prep.: op. cit.) have documented west to southwesterly sediment transport in the Mamadawerre Sandstone, and mainly southerly transport in younger parts of the Subgroup. Thin intervals of thinner-bedded sandstone with an abundance of symmetrical ripple marks in the younger parts in Milingimbi may be marine sands, as they display bipolar (SW–NE) currents, but Carson et al. (in prep.) interpret these intervals as possibly the product of distal sandy flood plains subject to sheet-flooding.

Tectonic setting

The Mamadawerre Sandstone and Nungbalgarri Volcanics (and equivalent volcanics; Fig. 27) vary markedly in thickness, and appear to be limited above by a regional unconformity. In the central southern Mount Evelyn 1:250 000 Sheet area (Stuart-Smith et al. 1988: ‘Stow Region, Northern Territory — 1:100 000

Geological Map Commentary', BMR [AGSO], Canberra), sedimentation of these units apparently was fault-controlled, for they thin rapidly from around 1500 m to zero over a few kilometres. It may be no coincidence that local depositional basins in which these units accumulated are closely related spatially to coarse clastic rocks and volcanics of the El Sherana and Edith River Groups, and hence may be closer in age to these groups. The younger components of the Subgroup, the Gumarrirnbang Sandstone and younger units, show no such abrupt thickness changes, and appear to blanket the older packages. The implications of this are that a phase of extension and local basin formation during El Sherana–Edith River Group–Mamadawerre Sandstone–Nungbalgarri Volcanics time preceded the development of a broader sag basin during the remainder of the Kombolgie Subgroup time, and that the unconformity at the top of the Edith River Group represents a time break of only a few million years.

Conclusions

The Kombolgie Subgroup is an appropri-

ate name for the collection of formations and members previously referred to as the 'Kombolgie Formation'. The Subgroup is constrained in age between 1822 Ma and probably 1730 Ma (certainly >1720 Ma), and is presumed to occupy only an earlier portion of that time interval. The recognition of a regional unconformity above the Nungbalgarri Volcanics and its equivalents offers scope for interpreting the older parts of the Subgroup as products of an extensional regime 1800 Ma or more ago, and the younger parts as sag basin deposits several to tens of millions of years younger. The lower parts were deposited in a mainly braided stream environment punctuated by brief intervals of marine deposition. Marine conditions predominated only at the top (McKay Sandstone), but thin intervals in the Gumarrirnbang and Marlgoa Sandstones may also be marine.

Whereas the stratigraphy of the Subgroup is now moderately well understood, it could be improved by a systematic reassessment of stratigraphic thickness variations. The palaeogeography during deposition is still poorly understood, and could be en-

hanced by a systematic palaeocurrent and facies study of the Subgroup. Much remains to be done in improving our understanding of the tectonic setting of the Subgroup, which appears to include elements of a lower extensional basin and an upper sag basin. Further studies could yield dividends both in terms of our understanding of the provenance of the sands, and of the tectonic setting into which these sands were deposited. An understanding of these features has not only intrinsic interest in terms of understanding the landscape features of Kakadu and Nitmiluk National Parks but would have practical application in minerals exploration in areas outside the parks.

¹ Minerals Division, Australian Geological Survey Organisation, GPO Box 378, Canberra, ACT 2601; tel. +61 2 6249 9307(IS), +61 2 6249 9597(AB); fax +61 2 6249 9956 (IS); email Ian.Sweet@agso.gov.au, Albert.Brakel@agso.gov.au

² Formerly the Northern Territory Geological Survey; currently Geoverde Pty Ltd, PO Box 479, Jamison Centre, ACT 2614; tel. and fax +61 2 6251 0845, email Icarson@geoverde.com.au.

Walpole et al. (1968)				Roberts & Plumb (1965)		Needham & Stuart-Smith (1985)				Carson et al. (in prep.); Sweet et al. (1999)	
				McKay Sandstone		McKay Sandstone				McKay Sandstone	
Kombolgie Formation	Henwood Creek *			Kombolgie Formation	Nungbalgarri*	Kombolgie Formation	Phk ₂ -		Kombolgie Subgroup	Marlgowa Sandstone	
	McAddens Creek, * Plum Tree Creek, * Birdie Creek, * and Nungbalgarri*						Henwood Creek * Gilruth *			Gilruth *	
	Kurrundie Member						'upper Kombolgie'			Gumarrirnbang Sandstone	
						McAddens Creek, * Birdie Creek, * and Nungbalgarri*				Nungbalgarri Volcanics	
						Phk ₁ -'lower Kombolgie'				Mamadawerre Sandstone	
Undivided Edith River Volcanics											
Edith River Volcanics	Phillips Creek Member	Pul Pul Rhyolite Member, Scinto Breccia Member	Hindrance Creek Member			Edith River Group	Plum Tree Creek Volcanics		Edith River Group		
							Phillips Creek, Hindrance Creek, and Kurrundie Sandstones				
						El Sherana Group	Tollis Formation	Big Sunday Fm	El Sherana Group		
								Pul Pul Rhyolite			
								Coronation Sst			
								Scinto Breccia			
										Finniss Group	Tollis Formation

16/NT/7

16/NT/611

Fig. 27. Past (first three columns) and present (last column) nomenclature of the Kombolgie unit and adjacent formations/members. Full names of units with an * is ... Volcanic Member. Note that the names McAddens Creek and Birdie Creek Volcanic Members are still applied to units in the Mount Evelyn and Katherine 1:250 000 Sheet areas.



The AGSO Research Newsletter is published twice a year, in May and November. The camera-ready copy for this issue was prepared by Lin Kay. Correspondence relating to the AGSO Research Newsletter should be addressed to Geoff Bladon, Editor, AGSO Research Newsletter, Australian Geological Survey Organisation, GPO Box 378, cnr Jerrabomberra Avenue & Hindmarsh Drive, Canberra, ACT 2609; tel. +61 2 6249 9111 (extn 9249) or 6249 9249 (direct), fax +61 2 6249 9984, e-mail gbladon@agso.gov.au. An electronic version of this newsletter is accessible on the WWW at <http://www.agso.gov.au/information/publications/resnews/>
© Commonwealth of Australia. ISSN 1039-091X

PP255003/00266